Journal of Inflammation Research

Dovepress
Taylor & Francis Group

Open Access Full Text Article

ORIGINAL RESEARCH

Bioinformatics-Based Exploration of the Ability of Ginkgetin to Alleviate the Senescence of Cardiomyocytes After Myocardial Infarction and Its Cardioprotective Effects

Han Li[1,*], Dongsheng Wei[2,*], Huimin Cao[2], Yelei Han[1], Luzhen Li[1], Yuting Liu[1], Jiajie Qi[1], Xinyue Wu[1], Zhe Zhang[2,3]

[1]The First School of Clinical Medicine, Liaoning University of Traditional Chinese Medicine, Shenyang, 110847, People's Republic of China; [2]Key Laboratory of Ministry of Education for TCM Viscera-State Theory and Applications, Liaoning University of Traditional Chinese Medicine, Shenyang, 110847, People's Republic of China; [3]Affiliated Hospital of Liaoning University of Traditional Chinese Medicine, Shenyang, 110032, People's Republic of China

*These authors contributed equally to this work

Correspondence: Zhe Zhang, Affiliated Hospital of Liaoning University of Traditional Chinese Medicine, No. 33 Beiling Street, Shenyang, 110032, People's Republic of China, Tel +86-18102459155, Email pedtrainzhzh7676@163.com

Journal of Inflammation Research downloaded from https://www.dovepress.com/
For personal use only.

Purpose: Myocardial infarction (MI) is a prevalent cardiovascular disorder affecting individuals worldwide. There is a need to identify more effective therapeutic agents to minimize cardiomyocyte damage and enhance cardioprotection. *Ginkgo biloba* extract is extensively used to treat neurological disorders and peripheral vascular diseases. The aim of this study was to determine the protective effects and mechanisms of ginkgetin on postinfarction cardiomyocytes through bioinformatics and experimental validation.

Methods: Bioinformatics analysis was performed to predict the underlying biological mechanisms of ginkgetin in the treatment of MI. Next, we performed further validation through experiments. For in vivo studies, we used coronary ligation to construct an MI rat model. In vitro, oxygen and glucose deprivation (OGD) was performed to simulate ischemia in H9c2 cardiomyocytes.

Results: Bioinformatics analysis revealed that the key targets of ginkgetin for MI treatment were MMP2, MMP9, and VEGFA. Immune infiltration analysis revealed that ginkgetin might be involved in immune regulation by acting on the TCR signaling pathway. The results of the GO enrichment analysis revealed that ginkgetin might protect the heart by acting on the cell membrane to alleviate the senescent apoptosis of cardiomyocytes after MI. In vivo studies revealed that ginkgetin ameliorated myocardial pathological damage and cardiac decompensation after MI. It also alleviated the inflammatory infiltration and senescent apoptosis of cardiomyocytes after MI. Additionally, ginkgetin can downregulate the activation signals of the TCR signaling pathway by dephosphorylating CD3 and CD28. In vitro studies revealed that ginkgetin attenuated elevated OGD-induced cytotoxicity, increased cell viability, and alleviated OGD-induced senescent apoptosis, thus protecting cardiomyocytes.

Conclusion: Ginkgetin inhibits postinfarction myocardial fibrosis and cardiomyocyte hypertrophy, scavenges oxygen free radicals, decreases postinfarction limbic cell inflammatory infiltration, suppresses activation of the inflammatory-immune pathway, and delays postinfarction peripheral cells from undergoing senescent apoptosis, thus protecting the heart.

Keywords: myocardial infarction, ginkgetin, senescence-associated secretory phenotype, immune infiltration, TCR signaling pathway

Introduction

Myocardial infarction (MI) is a major cardiovascular disease worldwide and is the primary cause of mortality globally; its prevalence is increasing among younger individuals.[1–3] According to clinical guidelines, restoring blood flow and minimizing myocardial damage are necessary steps for MI treatment.[4] However, the mortality rate for patients experiencing cardiogenic shock after MI decreases by only 8.3% after conventional surgical and pharmacological interventions are applied.[5] As cardiomyocytes are highly differentiated terminal cells with negligible proliferative capacity in adulthood, the loss of

Received: 14 August 2024
Accepted: 21 December 2024
Published: 7 January 2025

© 2025 Li et al. This work is published and licensed by Dove Medical Press Limited. The full terms of this license are available at https://www.dovepress.com/terms.php and incorporate the Creative Commons Attribution – Non Commercial (unported, v3.0) License (http://creativecommons.org/licenses/by-nc/3.0/). By accessing the work you hereby accept the Terms. Non-commercial uses of the work are permitted without any further permission from Dove Medical Press Limited, provided the work is properly attributed. For permission for commercial use of this work, please see paragraphs 4.2 and 5 of our Terms (https://www.dovepress.com/terms.php).

Graphical Abstract

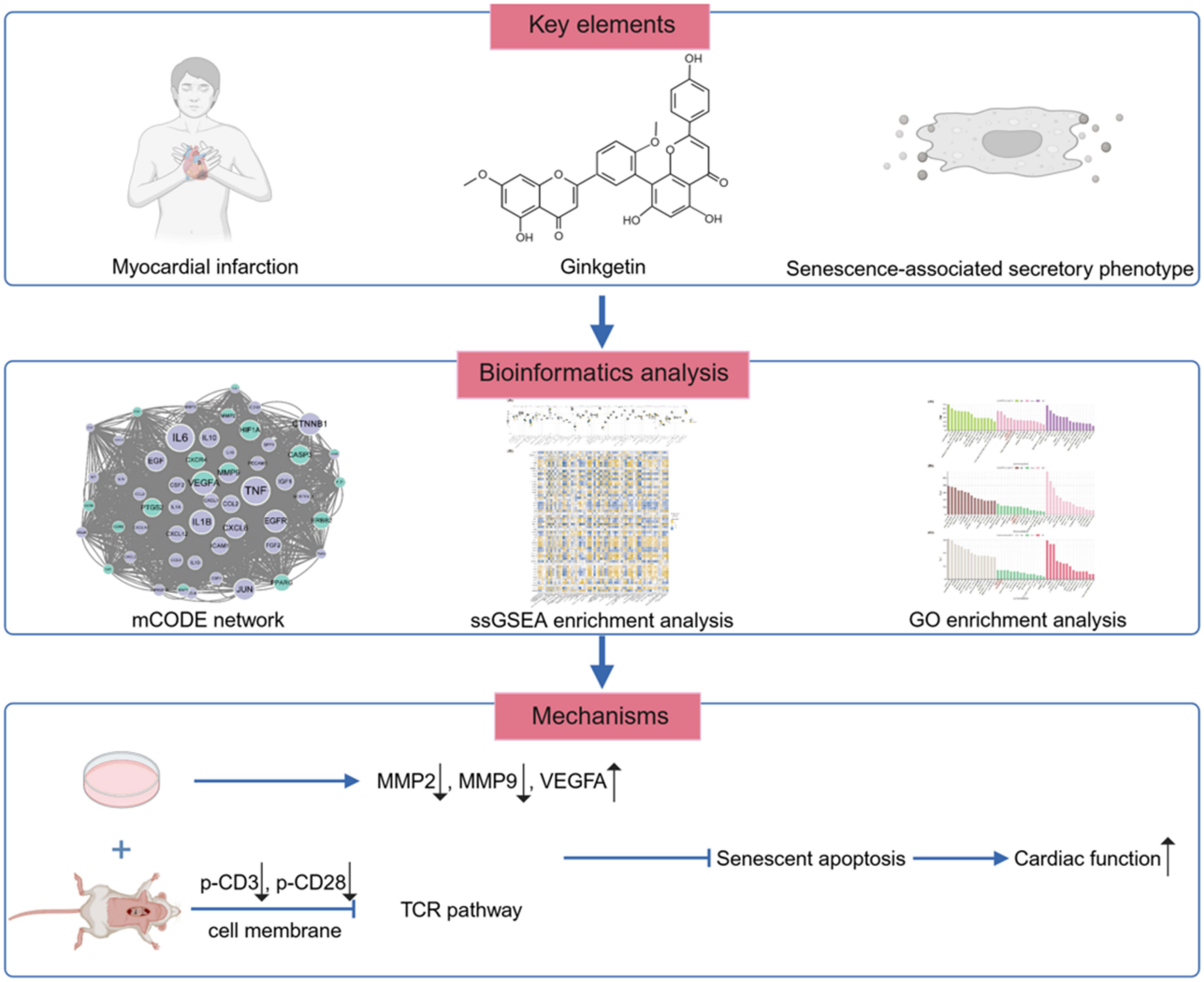

cardiomyocytes due to MI is irreversible.[6] Thus, identifying more effective therapeutic agents to minimize cardiomyocyte damage and enhance cardioprotection is necessary for improving the prognosis of MI patients.

Cellular senescence, characterized by irreversible cell cycle arrest due to damage at the molecular level, is commonly associated with "replicative senescence".[7] Recent studies have shown that senescent cells can maintain metabolic activity, contributing to senescence through autocrine secretion and affecting the microenvironment via the paracrine secretion of growth factors, chemokines, and proteases. This results in the induction of senescence in peripheral cells.[8–10] The stable arrest and secretion of biologically active compounds by these cells is referred to as the senescence-associated secretory phenotype (SASP).[7]

Following MI, hypoxia-induced and ischemia-induced necrosis of cardiomyocytes at the infarction site leads to the emergence of SASP cardiomyocytes at the infarct margins. The accumulation of senescent cells and the extensive release of inflammatory factors trigger a sustained inflammatory cascade in bordering cardiomyocytes.[11,12] Inflammatory factors act on peripheral cells in a paracrine manner, promoting the migration and proliferation of immune cells, continuously activating the inflammatory-immune pathway, and placing ventricular cells in a state of immune infiltration. This exacerbates the loss of borderline infarcted cardiomyocytes and their senescent apoptosis.[13–15]

Traditional Chinese medicine is an important source of modern drug discovery and development.[16] *Ginkgo biloba*, which is native to China, is widely recognized for its disease-resistant leaves and is cultivated for medicinal and ornamental purposes.[17] In the last century, Schwabe Pharmaceuticals in the former Federal Republic of Germany developed EGb761, a high-purity *Ginkgo biloba* extract (GBE), which is widely used to treat neurological and peripheral vascular diseases.[18] GBE has anti-inflammatory, antiplatelet aggregation, antioxidative, and antiaging properties.[19] The main component of EGb761 was ginkgetin (24%). An increasing number of studies have indicated that ginkgetin has remarkable anti-inflammatory, anti-apoptotic, and hypolipidemic effects, potentially making it a promising candidate for the treatment of cardiovascular diseases such as atherosclerosis.[20,21] Despite extensive research on ginkgetin, little is known about its role in the treatment of myocardial infarction. Notably, ginkgetin alleviates the aging phenotype in aged mouse models and inhibits abnormally activated STING signaling pathways.[22] We used bioinformatics to identify the key targets, signaling pathways, and immunological mechanisms of ginkgetin treatment in MI rats and verified them via in vivo animal experiments and in vitro cellular experiments to assess the role of ginkgetin in mitigating senescent apoptosis in cardiac myocytes after MI and in protecting the heart.

Materials and Methods

Bioinformatics Analysis

Screening of Genes Targeted for Drugs, Diseases, and Phenotypes

The target genes of ginkgetin, the main component in GBE, were screened from seven databases: the Comparative Toxicogenomics Database (CTDbase), Swiss Target Prediction, the Binding Database Home, DrugBank, ChEMBL, SuperPred, and the Similarity Ensemble Approach (SEA). When databases displayed only the full name of a gene, these names were converted into their corresponding English abbreviations via the String and UniProt databases. Concurrently, disease ontology (DO) enrichment analysis was performed to assess the involvement of these drug target genes in cardiovascular diseases. Three MI gene datasets, namely, GSE34198,[23] GSE48060,[24] and GSE97320,[25] were obtained from the Gene Expression Omnibus (GEO) database, with peripheral blood serving as the source for all three datasets. SASP target genes were obtained from the Web of Science (WOS).[26] Finally, common genes (CGs) at the intersection of SASP and MI were identified for further analysis. All public database procedures involving human data were approved by the Ethics Committee of the Affiliated Hospital of Liaoning University of Traditional Chinese Medicine (Ethics No. Y2024298CS (KT) −298-01).

Constructing a Drug-Disease-Phenotype mCODE Network

The common target genes of ginkgetin and CGs were identified by merging CGs with drug target genes. Additionally, a protein-protein interaction (PPI) network map was constructed using the STRING database (STRING: functional protein association networks, string-db.org). PPI network maps emphasizing centrality size were generated using the cytoNCA plugin in Cytoscape, and drug target and disease-associated genes were differentiated by distinct colors. Using the mCODE plugin, the most significant subgroups were identified via the following parameters: degree cutoff = 2, node score cutoff = 0.2, K-core = 2, and maximum depth = 100. Genes within this core subgroup were designated "keycluster" genes.

Immune Infiltration Analysis

The infiltration of 63 immune cells/functions associated with MI was analyzed through single-sample gene set enrichment analysis (ssGSEA). The "vioplot" package was used to compare and visualize the levels of immune infiltration between the MI and healthy groups. This tool also facilitated the analysis of the correlations and differences between the expression levels of key cluster genes and immune cells/functions. This approach helps identify the core immune cells/functions that play a significant role in the treatment of MI with ginkgetin.

Gene Ontology (GO) Enrichment Analysis

GO enrichment analysis was conducted in R for drug target genes, CGs, and key cluster genes, integrating the top 15 biological processes (BP), cellular components (CC), and molecular functions (MF) across the three enrichments. This analysis revealed the underlying biological mechanisms of ginkgetin treatment for MI by examining the intersections among these three sets of enrichment results.

https://doi.org/10.2147/JIR.S491535

Animal Preparation, Modeling, and Drug Administration

In total, 40 SD rats were allocated to two groups, seven to the sham operation group and 33 to the modeling group, based on a random number method. Following acclimation for one week, coronary artery ligation of the left anterior descending branch was performed on the eighth day under anesthesia induced by an intraperitoneal injection of sodium pentobarbital. During surgery, specialized respiratory support and heating pads ensure animal safety. The chests of the rats in the sham-operated group were opened without performing ligation. To prevent infection, postoperative intramuscular penicillin was administered for three consecutive days. After transcoronary ligation, 28 rats successfully underwent the modeling procedure. The 28 rats were subsequently divided into four groups, namely, the MI model group, the metoprolol (ZOK) group, the low-dose GBE (Schwabe, Germany) group, and the high-dose GBE group, each containing seven rats, using the random number method. Starting on the fourth day after the operation, 2.5 mg/kg/day ZOK was administered to the ZOK group, 50 mg/kg/day GBE was administered to the GBE low-dose group, and 200 mg/kg/day GBE was administered to the GBE high-dose group; the same volume of saline was administered to the sham-operated and model groups. After six weeks of continuous gavage, blood was collected from the abdominal aorta under anesthesia with sodium pentobarbital, and the hearts were removed postmortem.

All SD rats were housed in an SPF-grade animal facility at Liaoning University of Traditional Chinese Medicine under natural lighting conditions at 23 °C±2 °C and 60–70% relative humidity. The rats had free access to food and water and were cared for according to the National Institutes of Health Guide for the Care and Use of Laboratory Animals (NIH Publication No. 8023, revised 1978). All animal experimental procedures were approved by the Animal Ethics Committee of Liaoning University of Traditional Chinese Medicine (Ethics No. 21000042023021). All in vivo experiments utilized male rats (8–-12 weeks old, weight: 180–220 g) obtained from Liaoning Changsheng Biotechnology Co., Ltd., under Animal License No. SCXK (Liao) 2020–0001.

Histopathological Observation of the Myocardium

The heart was longitudinally bisected along the ligature in the sagittal plane. One half was used for paraffin sectioning, and the other half was used for frozen sectioning. The myocardial tissue intended for paraffin sectioning was fixed in 4% paraformaldehyde for 24 h, embedded in paraffin, and then cut into thin sections (4 μm thick). Histopathological changes in the myocardium were examined via hematoxylin and eosin (H&E) staining, Sirius Red staining, and Masson's trichrome staining. Images captured in the visual field of Sirius Red-stained sections and Masson-stained sections were used to analyze the area of collagen fibers.

Pathological Observation of Myocardial Microstructure

Fresh myocardial tissue was sectioned into 1 mm^3 pieces and fixed in 2.5% glutaraldehyde solution for 24 h, followed by fixation in a 1% osmium fixative for 2 h. The samples were then dehydrated using a graded series of acetone and embedded using conventional electron microscopy techniques. The sections were cut to a thickness of 50 nm. Microstructural alterations in the myocardium were observed using transmission electron microscopy after double staining with uranyl acetate and lead citrate.

Echocardiography

The rats were anesthetized and fixed on an ultrasound platform. After skin preparation, the left ventricular ejection fraction (LVEF), left ventricular short-axis shortening (LVFS), left ventricular end-diastolic diameter (LVEDD), and left ventricular end-systolic diameter (LVESD) were detected using M-mode ultrasound to evaluate LV function.

Enzyme-Linked Immunoassay (ELISA) for Serum NT-proBNP, IL-6, IL-1β, and TNF-α Levels

ELISA was performed to determine the levels of serum amino-terminal brain natriuretic peptide precursor (NT-proBNP), interleukin-6 (IL-6), interleukin-1β (IL-1β), and tumor necrosis factor-α (TNF-α) in the rats. The OD values were measured at 450 nm using an enzyme marker following the manufacturer's instructions.

Wheat Germ Agglutinin (WGA) Fluorescence Staining

The paraffin sections were deparaffinized in water, placed in an EDTA antigen repair solution for antigen repair, washed three times with phosphate buffer solution (PBS), and shaken dry. WGA staining solution was added dropwise, and the sections were incubated for 30 min at 37 °C in the dark. Then, the sections were blocked with an anti-fluorescence quenching sealer. Cells (n = 15) were randomly selected from each section in each group to quantify the average cardiomyocyte area (μm^2), and the cell area was quantified using ImageJ.

ROS Fluorescence Staining

The frozen sections were rewarmed and dried. A histochemical pen was used to draw a circle around the tissue. Next, ROS stain and DAPI stain were added sequentially, after which the sections were placed in PBS, washed three times on a decolorizing shaker, and then sealed with a drop of anti-fluorescence quenching sealer after the water was controlled. Statistical analyses were performed using ImageJ.

TUNEL Fluorescence Staining

The paraffin-embedded sections were deparaffinized in water. After the TUNEL reaction mixture was added dropwise, the nuclei were restained. The sections were subsequently placed in PBS and washed three times on a decolorizing shaker. An anti-fluorescence quenching agent was added to the sealed samples, and statistical analysis was conducted using ImageJ.

Immunohistochemical (IHC) Staining to Detect p53 and p21 Expression in the Myocardium

The paraffin sections were deparaffinized in water, and after antigen retrieval, primary antibodies were added and incubated overnight at 4 °C. The samples were washed with PBS, and secondary antibodies were added dropwise to incubate for 1 h. Color was developed using DAB, followed by hematoxylin restaining. The expression of p53 and p21 in each group of sections was observed under an ordinary light microscope.

β-Galactosidase Staining of Rat Myocardial Tissue

The frozen sections were incubated with β-gal fixative, fixed at room temperature for 15 min, and washed with PBS three times. After the PBS was aspirated, the sections were immersed in the prepared staining working solution and incubated at 37 °C overnight. The sections were observed under an ordinary light microscope and statistically analyzed using ImageJ.

Immunofluorescence (IF) Staining to Detect Changes in p-CD3 Expression

After the frozen sections were washed with PBS, 0.5% Triton X-100 was added dropwise, and the samples were incubated at room temperature for 15 min to disrupt the membrane. Then, the sections were blocked for 30 min in 5% BSA in a 37 °C water bath and incubated with p-CD3 primary antibodies at 4 °C overnight. The fluorescent secondary antibodies were subsequently added dropwise and incubated at 37 °C for 1 h. After the nuclei were stained with DAPI, the slices were blocked, and statistical analysis was performed using ImageJ.

Fluorescence Quantitative Polymerase Chain Reaction (RT-qPCR)

In total, 0.5 cm of myocardial tissue around the infarcted area was thawed and homogenized. The TRIzol method was used to extract total RNA, which was reverse-transcribed into cDNA. The cDNA obtained was used as a template to quantitatively amplify the target genes MMP2, MMP9, and VEGFA and the internal reference gene GAPDH. RT-qPCR was performed under the following amplification conditions: predenaturation at 95 °C×30 s, amplification at 95 °C for 10 s and 60 °C for 30 s for a total of 40 cycles, and extension at 72 °C for 2 min. The relative ratio of the target gene to GAPDH was used for expression, and the relative ratio was calculated via the $2^{-\Delta\Delta Ct}$ method. The primer sequences are shown in Table 1.

Table 1 Sequences of Primers

mRNA	Primer Sequence (5'–3')	
VEGFA	Forward:	GCAGCGACAAGGCAGACTATTC
	Reverse:	TGAGGGAGTGAAGGAGCAACC
MMP9	Forward:	CATGCGCTGGGCTTAGATCA
	Reverse:	GAGGCCTTGGGTCAGGTTTAGAG
MMP2	Forward:	TTTGGTCGATGGGAGCATGG
	Reverse:	ATAGCTGTGACCACCACCCT
GAPDH	Forward:	TCTCTGCTCCTCCCTGTTCT
	Reverse:	TACGGCCAAATCCGTTCACA

Western Blotting Detection of Rat Myocardial Tissue

First, 0.5 cm of myocardial tissue around the area of MI was collected from each group of rats. The tissue was ground in liquid nitrogen and lysed by adding RIPA lysis buffer. The mixture was subsequently centrifuged at 4 °C and 12000 rpm for 15 min. Next, the supernatant was aspirated, and the protein concentration was detected via the BCA method. Subsequently, 5× loading buffer and lysis buffer were added to determine the protein concentration, and protein denaturation was performed at 95 °C for 5 min. The proteins were separated via sodium dodecyl sulfate-polyacrylamide gel electrophoresis (SDS-PAGE), followed by wet transfer to a PVDF membrane. The samples were blocked with 5% skim milk powder or 5% BSA at room temperature, after which they were incubated with primary antibodies against MMP2 (1:1000, Wanlei, Shenyang, China), MMP9 (1:1000, Wanlei, Shenyang, China), VEGFA (1:1000, Wanlei, Shenyang, China), cleaved-caspase 3 (1:750, Wanlei, Shenyang, China), Bax (1:750, PTM, Hangzhou, China), Bcl-2 (1:1000, Bioss, Beijing, China), PD1 (1:1000, Wanlei, Shenyang, China), p-CD28 (1:1000, Affinity, Jiangsu, China), CD28 (1:1000, Affinity, Jiangsu, China), p-PI3K (1:1000, Affinity, Jiangsu, China), PI3K (1:1000, Affinity, Jiangsu, China), p-AKT (1:1000, Affinity, Jiangsu, China), AKT (1:1000, Affinity, Jiangsu, China), p-NFκB p65 (1:750, Wanlei, Shenyang, China), NFκB p65 (1:1000, Affinity, Jiangsu, China), GAPDH (Epizyme, 1:3000, Shanghai, China), and β-actin (1:1000, Wanlei, Shenyang, China) overnight at 4 °C on a shaker. The following day, the membrane was incubated with secondary antibodies at room temperature for 1 h, after which the ECL chromogenic solution was added dropwise to the PVDF membrane for protein banding. The gray values of the bands were analyzed using ImageJ.

Cell Culture, Oxygen-Glucose Deprivation (OGD), and Drug Administration

H9c2 cardiomyocytes were purchased from the Procell Cell Bank and cultured in high-sugar DMEM supplemented with 10% fetal bovine serum and 1% penicillin-streptomycin solution containing 95% air and 5% CO_2 in an incubator at 37 °C. The cells used in all subsequent experiments were in the logarithmic growth phase.

H9c2 cardiomyocytes were exposed to OGD in vitro to simulate myocardial ischemia-hypoxia. The high-glucose medium for normally cultured H9c2 cells was replaced with sugar-free DMEM and placed in a triple-gas incubator containing 94% N_2, 5% CO_2, and 1% O_2 for OGD modeling for 6 h. Unless otherwise indicated, ginkgetin (Yuanye, Shanghai, China) was added at a dose of 75 μM to the OGD-modeled cells for 6 h. Normally, cultured cells served as controls.

Cell Counting Kit-8 (CCK-8) Assay

H9c2 cardiomyocytes were inoculated in 96-well plates at a density of 1×10^4, and after wall attachment in normal culture, OGD modeling was conducted for 2 h, 4 h, 6 h, 8 h, 10 h, 12 h, and 24 h, after which the medium in the 96-well plates was discarded. The cells were rinsed with PBS once, and 100 μL of high-glucose medium containing 10 μL of CCK8 solution was added to each well of the plates. The cells were incubated in an incubator at 37 °C for 30 min in the dark, and the absorbance was measured at 450 nm using an enzyme marker.

Lactate Dehydrogenase (LDH) Secretion Assay

H9c2 cardiomyocytes were inoculated in 96-well plates at a density of 1×10^4, and OGD modeling was conducted as described in Section 2.16. The supernatant was transferred to a new 96-well plate, and cytotoxicity was assessed using an LDH kit following the manufacturer's instructions. Finally, the absorbance was measured at 490 nm using an enzyme marker.

Immunofluorescence (IF) Staining to Detect Changes in MMP2, MMP9, VEGFA, p21 and p53 Expression

H9c2 cells were cultured in 15 mm confocal Petri dishes. They were subjected to OGD modeling and drug administration for 6 h and washed three times with PBS. The membrane was disrupted by adding 0.5% Triton X-100 and incubated at room temperature for 15 min. Then, 5% BSA was added, and the mixture was placed in a 37 °C water bath and incubated for 30 min. MMP2, MMP9, VEGFA, p21, and p53 primary antibodies were added dropwise, after which the mixture was incubated at 4 °C overnight. Subsequently, fluorescent secondary antibodies were added dropwise, and the samples were incubated at 37 °C for 1 h. The sections were blocked after the nuclei were stained with DAPI. Photographs were taken using a laser scanning confocal microscope and statistically analyzed using ImageJ.

Western Blotting Detection of H9c2 Cardiomyocytes

H9c2 cells were subjected to OGD modeling and drug administration for 6 h. The cells were collected via trypsin digestion, washed with precooled PBS at 4 °C, and resuspended in lysis buffer. The remaining steps were the same as those described in Section 2.14. The primary antibodies (cleaved-caspase 3, Bax, and Bcl-2) were incubated with the samples overnight at 4 °C in a shaker.

β-Galactosidase Staining of H9c2 Cardiomyocytes

H9c2 cells were cultured in six-well plates for OGD modeling and drug administration for 6 h. After the medium was discarded, the cells were washed with PBS, followed by the addition of 1 mL of β-gal fixative per well, after which they were fixed for 15 min at room temperature and washed with PBS three times. The PBS was aspirated, and 1 mL of staining work-up solution was added to each well. A cling film was used to seal the six-well plates, which were incubated at 37 °C overnight. Observations were made under a light microscope, and statistical analyses were performed using ImageJ.

Statistical Analyses

Statistical analyses were performed using R (version 4.1.3). The threshold of significance for ssGSEA immune infiltration analysis and GO enrichment analysis was $P < 0.05$. SPSS (version 27) and GraphPad Prism (version 8) were used to analyze the experimental data, and the data are expressed as the means ± standard deviations (means ± SDs). The differences among multiple groups were determined by one-way analysis of variance (ANOVA), and all differences were considered statistically significant at $P < 0.05$.

Results

Results of Bioinformatics Analysis

Screening Results of Drug, Disease, and SASP-Targeting Genes

The initial step involved the screening of drug-targeting genes, identifying the target genes of ginkgetin across multiple databases: seven in CTDbase, 39 in Swiss Target Prediction, 11 in the binding database, eight in DrugBank, 254 in ChEMBL, 122 in SuperPred, and 56 in SEA, which summed to 422 unique drug-targeting genes after duplicates were eliminated. The DO enrichment analysis revealed that ginkgetin was enriched in atherosclerosis, which also implied that ginkgetin might play a protective role in the cardiovascular field (Figure 1A and B). Disease-targeting genes were subsequently screened by extracting genes from three datasets: GSE34198, GSE48060, and GSE97320. After removing duplicates, a total of 17,267 unique genes were obtained. The final step involved extracting SASP genes from WOS, and 125 phenotype-targeted genes were identified.

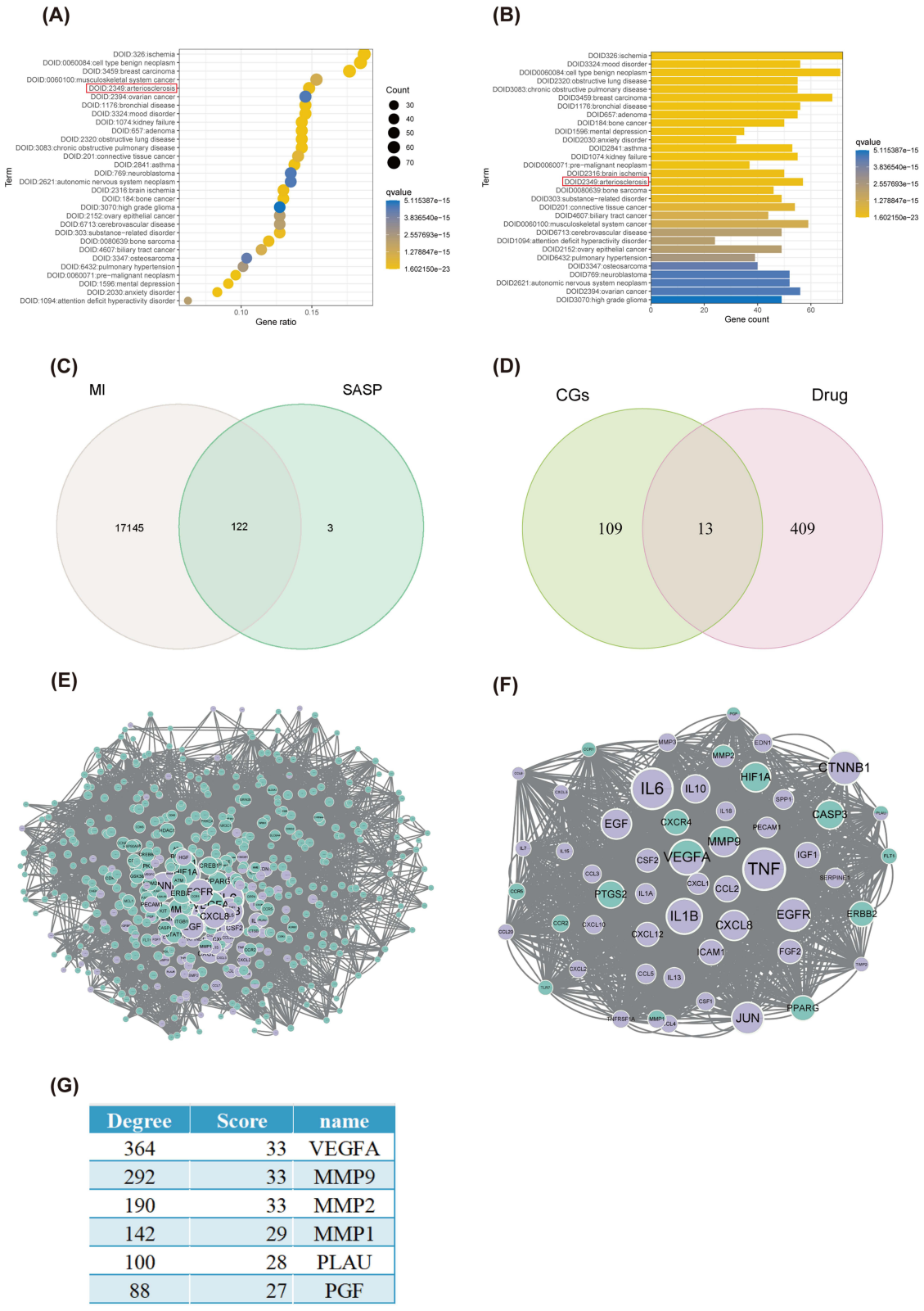

Degree	Score	name
364	33	VEGFA
292	33	MMP9
190	33	MMP2
142	29	MMP1
100	28	PLAU
88	27	PGF

Figure 1 Results of screening for drug, disease, and SASP target genes and mCODE network construction. (**A**) Bubble plot of the results of the DO enrichment analysis sorted by the number of enriched genes. The red box shows that ginkgetin is enriched in atherosclerosis. (**B**) A bar graph of the results of the DO enrichment analysis sorted by P value. The red box shows that ginkgetin is enriched in atherosclerosis. (**C**) Venn diagram of MI genes intersecting with SASP genes. (**D**) Venn diagram of CGs intersecting with drug target genes. (**E**) PPI protein interaction network diagram. (**F**) mCODE coregulation network diagram. (**G**) mCODE network Ginkgetin-CGs key gene score ranking.

Results of mCODE Network Construction

Fusing disease and SASP gene data resulted in the identification of 122 CGs (Figure 1C). After CGs were merged with drug target genes and duplicates were eliminated, 531 genes were identified (Figure 1D). A PPI network map was subsequently constructed using the STRING website (Figure 1E). A PPI network was generated via the cytoNCA plugin in Cytoscape, with centrality size as a criterion. The highest-scoring gene network subgroup, comprising 53 key cluster genes in this subgroup (Figure 1F), was then identified via the mCODE plugin. This subgroup has six ginkgetin-CGs key genes, including MMP2, MMP9, VEGFA, MMP1, PLAU, and PGF (Figure 1G). Three of the most relevant genes, MMP2, MMP9, and VEGFA, were selected on the basis of degree and score ranking.

Results of ssGSEA

The ssGSEA method was used to evaluate the characteristics of 63 immune cells/functions and to identify differences between the MI and normal groups. The results revealed significant differences in 49 immune cells/functions, primarily characterized by T-cell co-suppression, between the MI and normal groups ($P < 0.05$) (Figure 2A). The correlations between key cluster genes and immune cells/functions were subsequently analyzed (Figure 2B). A comparison of the numbers of *, **, and *** genes revealed nine genes associated with activation and 16 genes associated with inhibition of the T-cell receptor (TCR) signaling pathway. Thus, ginkgetin may contribute to cardioprotection after MI by mitigating the senescent apoptosis of cardiomyocytes by inhibiting the activation of the TCR signaling pathway.

Results of the GO Enrichment Analysis

GO enrichment analysis of drug target genes (Figure 3A), CGs (Figure 3B), and key cluster genes (Figure 3C) revealed specific patterns in CC, where both membrane rafts and membrane microdomains were enriched across drug targets, CGs, and key cluster genes. However, no significant enrichment was observed in BP or MF across the three analyses up to the intersection node (Figure 3A-C). These findings suggest that ginkgetin may exert cardioprotective effects by targeting the cell membrane and thus mitigate the senescent apoptosis of cardiomyocytes following MI.

Ginkgetin Ameliorates Myocardial Pathological Damage After MI

Coronary ligation was performed to induce MI in SD rats, followed by a six-week treatment regimen involving gavage of GBE. Histopathological changes in the myocardium were assessed via H&E staining, Sirius Red staining, Masson staining, and transmission electron microscopy (TEM). The H&E staining results indicated that in the sham-operated group, cardiomyocytes displayed uniform staining with a regular morphology, tight arrangement, centrally located rounded nuclei, and no cellular gaps or inflammatory infiltration. In contrast, cardiomyocytes in the model group exhibited edema, disorganized arrangement, increased cellular gaps, unevenness, shrinkage, strain, and mild inflammatory infiltration. Compared with the model group, both the ZOK group and various GBE-treated groups presented reduced cardiomyocyte edema, increased regular arrangement, and decreased inflammatory infiltration, with the greatest improvements recorded in the high-dose GBE group (Figure 4A). Sirius Red staining revealed that, relative to that in the sham-operated group, the normal myofibrillar tissue (yellow) in the model group was markedly decreased and supplanted by collagen fiber (red) deposition. However, the ZOK-treated and GBE-treated groups, especially the high-dose GBE group, presented significantly decreased MI-induced collagen fiber deposition (Figure 4B and E). Similarly, Masson staining revealed a significant decrease in collagen fiber (blue) deposition postinfarction in the ZOK- and GBE-treated groups (Figure 4C and F). TEM examination further revealed that, compared with those in the sham-operated group, myogenic fibers in the model group were disrupted, with marked and sparse mitochondrial swelling and the disappearance of mitochondrial cristae. In comparison, the GBE-treated groups presented neatly aligned myogenic fibers, significantly reduced mitochondrial swelling, and denser mitochondrial cristae (Figure 4D). These findings indicate that ginkgetin can mitigate myocardial pathological injury post-MI in rats.

Ginkgetin Improves Cardiac Decompensation After MI

To investigate the effect of ginkgetin on cardiac function following MI in rats, echocardiography, ELISA, and WGA staining were performed. Compared with those in the sham-operated group, the LVEF and LVFS were significantly lower

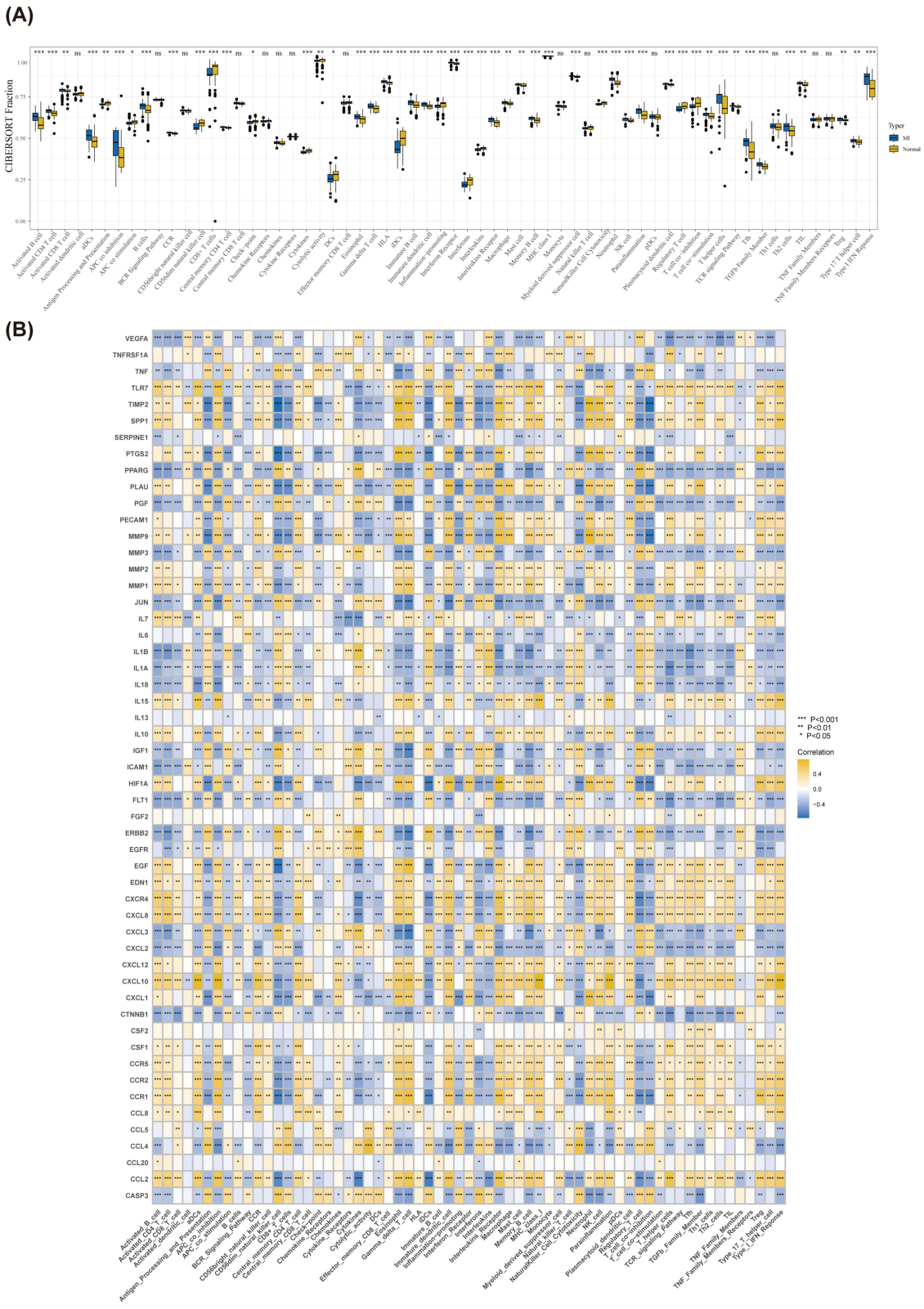

Figure 2 Results of ssGSEA. (**A**) Box plot of differential immunodiffusion. (**B**) Heatmap of the immunodiffusion of key cluster genes; * $P < 0.05$, ** $P < 0.01$, and *** $P < 0.001$.

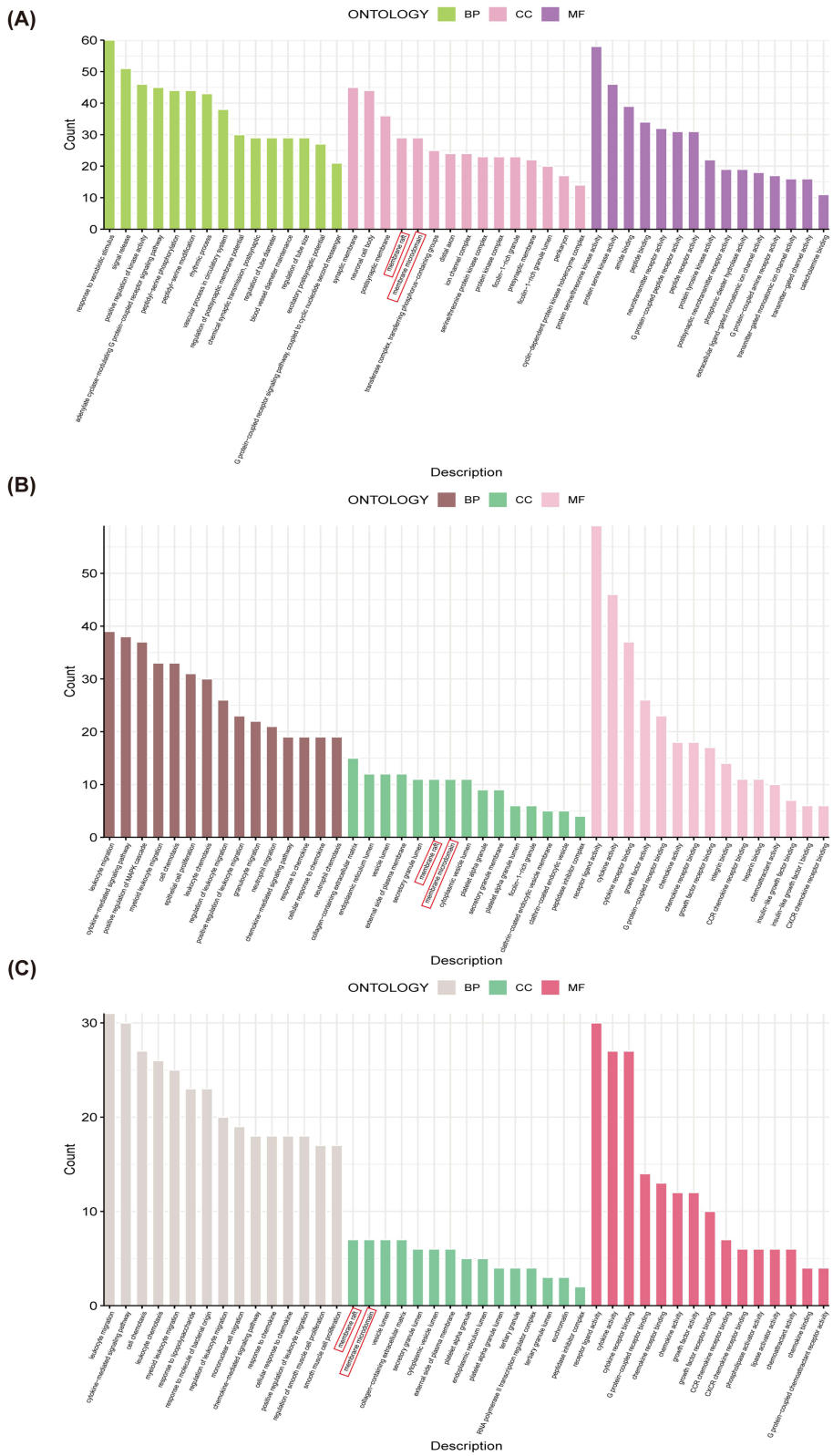

Figure 3 Results of the GO enrichment analysis. (**A**) A histogram of drug target genes GO enrichment analysis results. The red box indicates that drug target genes are enriched in membrane rafts and membrane microdomains. (**B**) A histogram of CGs GO enrichment analysis results. The red box indicates that CGs are enriched in membrane rafts and membrane microdomains. (**C**) A histogram of key cluster genes GO enrichment analysis results. The red box indicates that key cluster genes are enriched in membrane rafts and membrane microdomains.

https://doi.org/10.2147/JIR.S491535

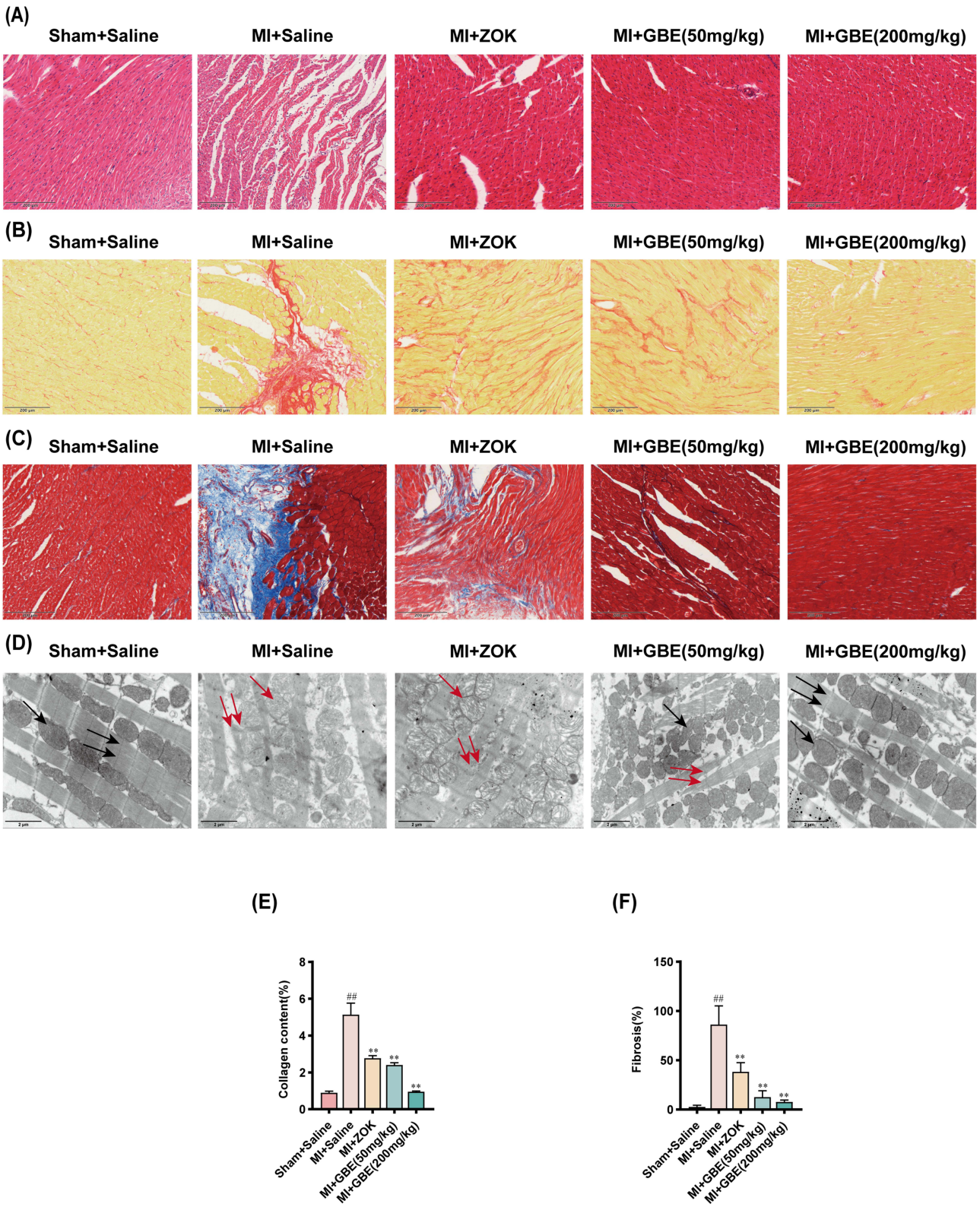

Figure 4 Ginkgetin ameliorates myocardial pathological injury after MI. (**A**) H&E staining results of the myocardial tissues of the rats in each group. (**B**) Sirius Red staining results for the myocardial tissues of the rats in each group. (**C**) Masson staining results of the myocardial tissues of the rats in each group. (**D**) Ultrastructural TEM examination of the myocardial tissues of the rats in each group; 5000×, scale bar = 2 μm. The black single arrows represent crista-structured dense mitochondria. The red single arrows indicate mitochondria with sparse cristae. The black double arrows represent myogenic fibers. The red double arrows indicate broken myogenic fibers. (**E**) Quantitative analysis of the collagen content via Sirius Red staining. (**F**) Macroscopic measurement of the fibrotic area via Masson staining. Longitudinal section × 200, scale bar = 200 μm; $^{\#\#}$ $P < 0.01$ compared with the sham-operated group; ** $P < 0.01$ compared with the model group. ($\bar{x}\pm s$, n = 3).

 https://doi.org/10.2147/JIR.S491535

in the model group, whereas the LVEDD and LVESD were significantly greater. Compared with the model group, the ZOK group presented a significant improvement in LVEF and a reduction in LVESD thickness, although no notable changes in LVFS or LVEDD were observed. The GBE dose groups showed significant improvements in LVEF and LVFS, along with reduced thicknesses of the LVEDD and LVESD (Figure 5A and B). ELISA revealed a significant increase in serum NT-proBNP levels in the model group compared with those in the sham-operated group, with notable reductions observed in the ZOK group and across all the GBE dose groups (Figure 5C). WGA staining revealed significant cardiomyocyte hypertrophy in the model group relative to the sham-operated group, whereas the number of cardiomyocytes was significantly lower in the ZOK and GBE dose groups (Figure 5D and E). As bioinformatics analysis revealed that MMP2, MMP9, and VEGFA were the genes associated with Ginkgetin-MI-SASP, RT-qPCR, and WB were conducted to assess the expression of these genes in myocardial tissues across the different rat groups. The results revealed that the expression of MMP2 and MMP9 was significantly lower in each GBE dose group than in the model group and that the expression of VEGFA was significantly greater in each GBE dose group than in the model group (Figure 5F–H). Therefore, ginkgetin can improve cardiac decompensation following MI, which highlights its high efficacy as a therapeutic agent in the management of post-MI cardiac dysfunction.

Ginkgetin Alleviates Inflammatory Infiltration and Senescent Apoptosis in Cardiomyocytes After MI

Following MI, the necrosis of cardiomyocytes in the infarcted area triggers a sustained inflammatory cascade bordering cardiomyocytes, leading to their senescent apoptosis. To elucidate the mechanism through which ginkgetin improves cardiac function postinfarction, various assays, including ROS staining, ELISA, TUNEL staining, WB, immunohistochemistry, and β-Galactosidase staining, were performed to determine the effects on inflammation, apoptosis, and senescence. Compared with the sham-operated group, the model group presented significantly greater fluorescence intensity of ROS. While the ZOK group presented no significant change in fluorescence intensity compared with the model group, the GBE dose groups presented a substantial decrease in ROS fluorescence intensity, particularly the high-dose group (Figure 6A and B). The ELISA results revealed that GBE at all doses significantly decreased the expression of the inflammatory factors IL-6, IL-1β, and TNF-α (Figure 6C). TUNEL staining revealed a significantly greater percentage of apoptotic cardiomyocytes in the model group than in the sham-operated group, and the percentage of apoptotic cardiomyocytes was significantly lower in the ZOK group and all the GBE dose groups (Figure 6D and E). The results of the WB assays revealed a decrease in the expression of the apoptosis markers cleaved caspase 3 and Bax and an increase in the expression of the anti-apoptotic marker Bcl-2 in the high-dose GBE group (Figure 6F and G). Immunohistochemistry revealed significantly greater expression of the senescence markers p21 and p53 in the model group than in the sham-operated group, with a significant reduction in their expression across all the GBE dose groups (Figure 7A and C). β-Galactosidase staining confirmed a lower positive rate of senescence in cardiomyocytes in the high-dose GBE group (Figure 7B and D). Therefore, ginkgetin attenuates inflammatory infiltration in cardiomyocytes at the infarct border and decreases the occurrence of senescent apoptosis in cardiomyocytes by scavenging ROS.

Ginkgetin Modulates T-Cell Signaling Pathway Activation for Cardioprotection

Bioinformatics predictions suggested that ginkgetin might confer cardioprotection by modulating the activation of the TCR signaling pathway. To test this hypothesis, IF staining was performed to assess the expression of p-CD3, a T-cell surface marker, in myocardial tissues from each rat group, and WB analysis was performed to evaluate the expression of proteins associated with the TCR signaling pathway. The IF staining results revealed a significantly greater p-CD3 fluorescence intensity in the model group than in the sham-operated group. The ZOK- and GBE-treated groups presented significantly lower fluorescence intensities than did the model group, with the lowest levels observed in the high-dose GBE group (Figure 8A and B). WB analysis revealed no significant difference in the expression of the negative T-cell surface regulatory factor PD1 across the groups (Figure 8C and E). However, the phosphorylation of CD28, a positive regulator on the T-cell surface, was significantly greater in the model group than in the control group; this finding indicated that the TCR signaling pathway was more active in the model group. This phosphorylation was significantly

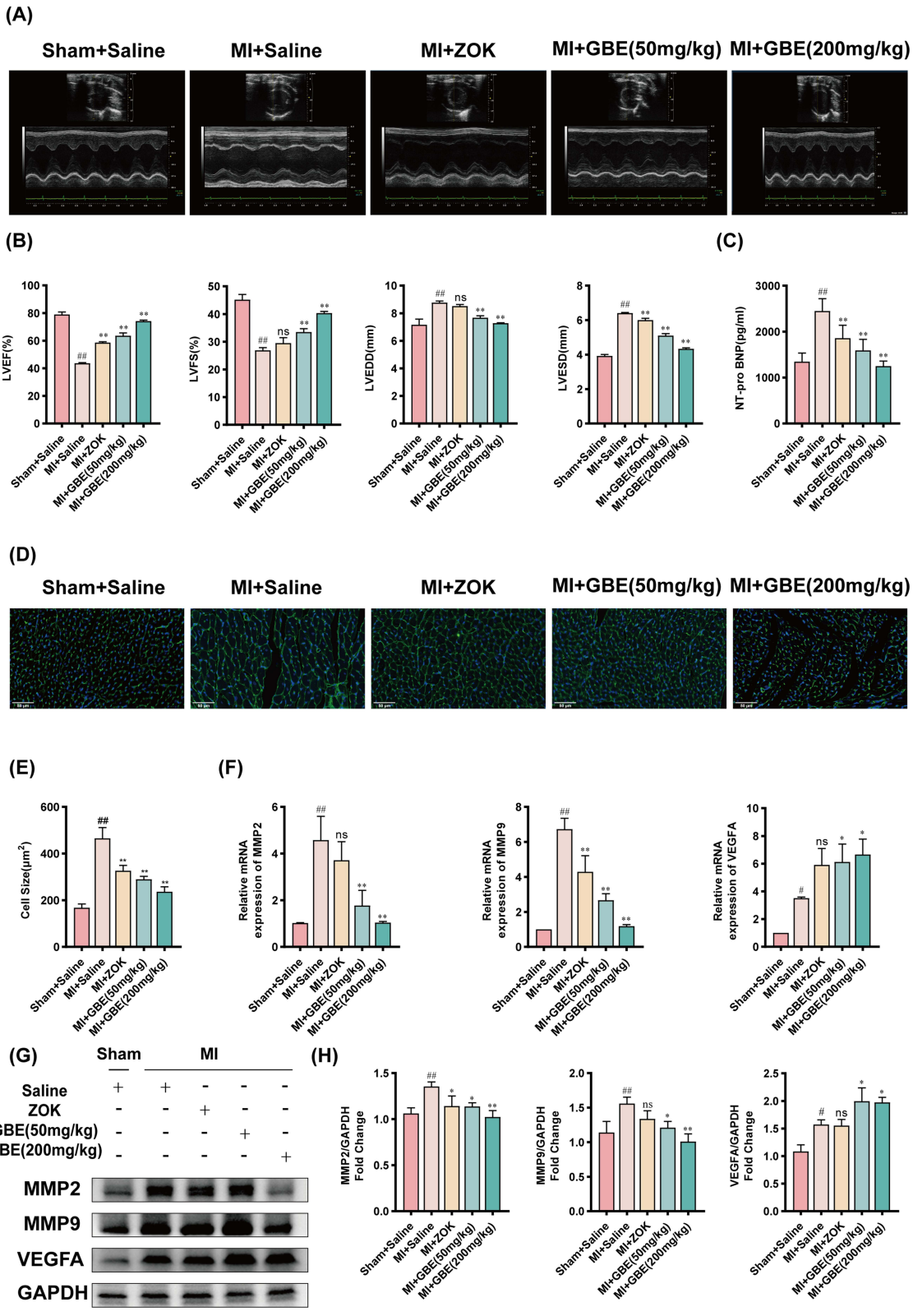

Figure 5 Ginkgetin ameliorates cardiac decompensation after MI. (**A**) M-mode ultrasound results of the rats in each group. (**B**) M-mode echocardiographic LVEF (%), LVES (%), LVEDD, and LVESD data of the rats in each group. (**C**) Differential histograms of the serum NT-pro BNP levels in the rats in each group ($\bar{x}$±s, n = 7). (**D**) WGA fluorescence staining results of rat myocardial tissue from each group. Longitudinal cut × 600, scale bar = 50 μm. (**E**) Differential histogram of the surface area of rat cardiomyocytes in each group. (**F**) Histogram of the relative expression of the MMP2, MMP9, and VEGFA mRNAs in the myocardial tissues of the rats in each group. (**G**) WB bands showing MMP2, MMP9, and VEGFA protein expression in the myocardial tissues of the rats in each group. (**H**) Quantitative analysis of MMP2, MMP9, and VEGFA expression in each group; $^{\#}$ $P < 0.05$ and $^{\#\#}$ $P < 0.01$ compared with the sham-operated group; * $P < 0.05$ and ** $P < 0.01$ compared with the model group ($\bar{x}$±s, n = 3).

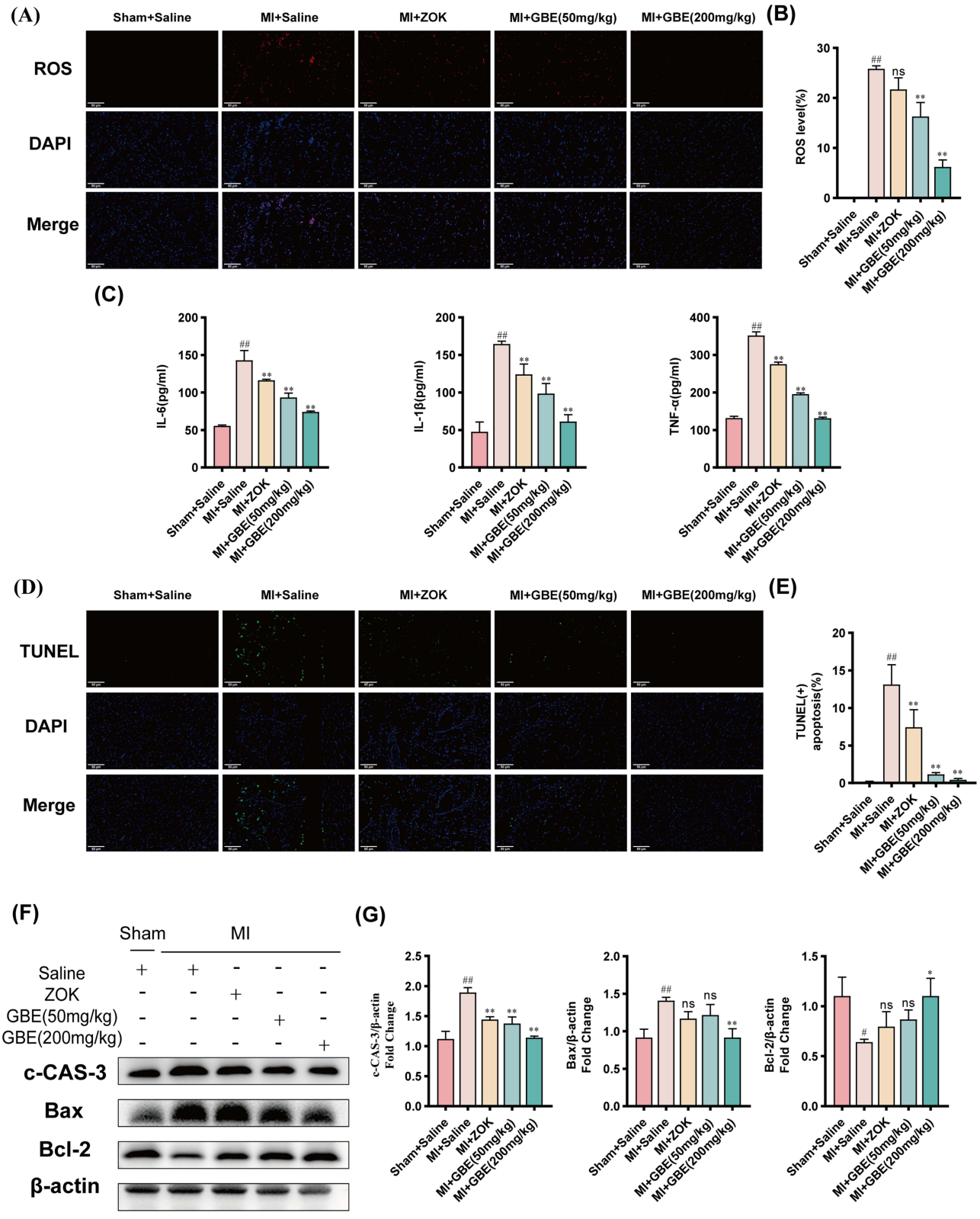

Figure 6 Ginkgetin alleviates inflammatory infiltration and apoptosis after MI. (**A**) Results of ROS staining of rat myocardial tissues from each group. Longitudinal section × 400, scale bar = 50 μm. (**B**) Quantitative analysis of ROS fluorescence intensity. (**C**) Differential histograms of the serum levels of the inflammatory factors IL6, IL-1β, and TNF-α in the rats in each group. ($\bar{x}$±s, n = 7). (**D**) TUNEL results of rat myocardial tissue from each group. Longitudinal section × 400, scale bar = 50 μm. (**E**) Quantitative analysis of the percentage of TUNEL-positive apoptotic cells. (**F**) WB bands showing cleaved caspase 3, Bax, and Bcl-2 protein expression in the myocardial tissues of the rats in each group. (**G**) Quantitative analysis of cleaved caspase 3, Bax, and Bcl-2 expression in each group; $^{\#}P < 0.05$ and $^{\#\#}P < 0.01$ compared with the sham-operated group; $^{ns}P > 0.05$, $^{*}P < 0.05$, and $^{**}P < 0.01$ compared with the model group ($\bar{x}$±s, n = 3).

https://doi.org/10.2147/JIR.S491535

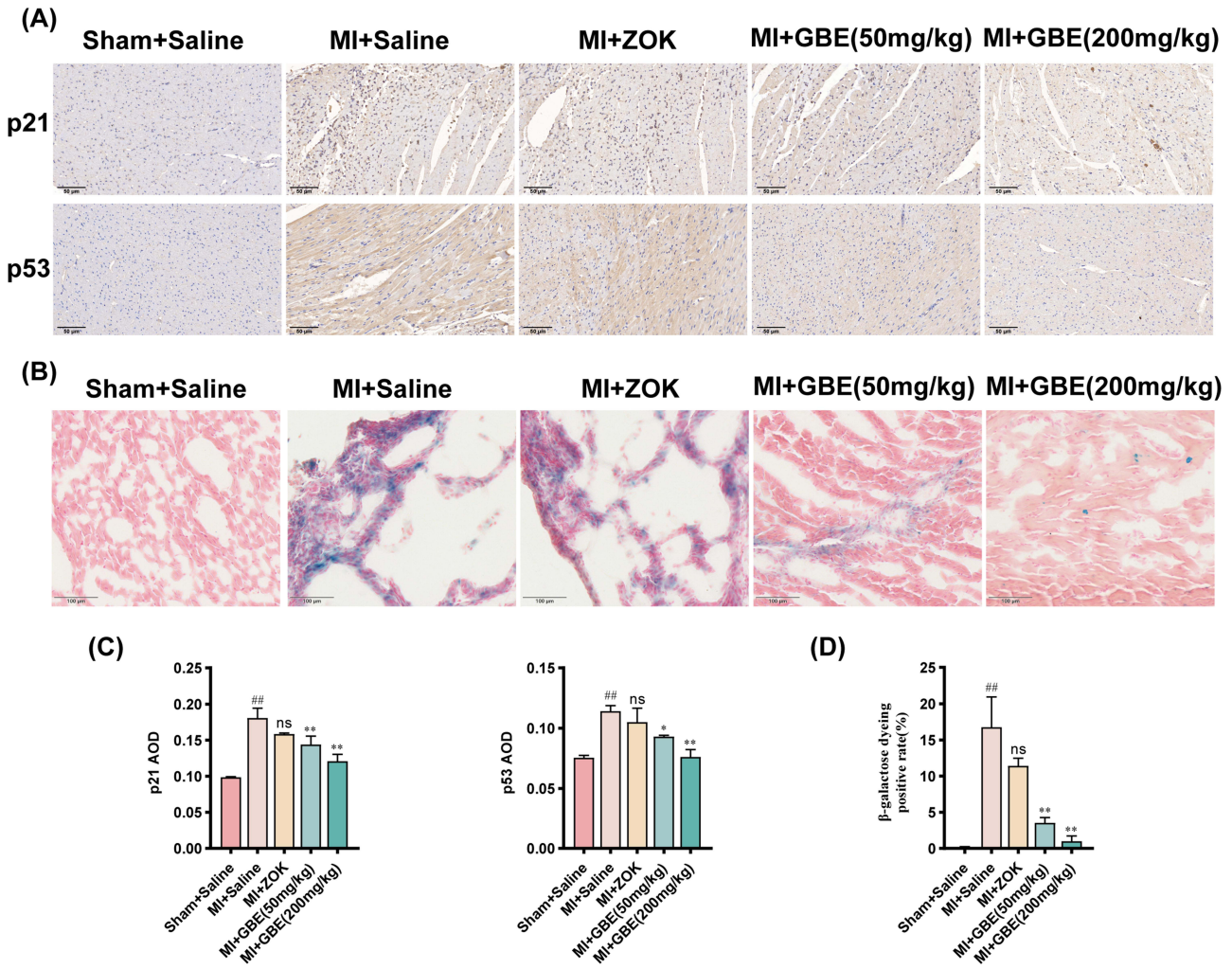

Figure 7 Ginkgetin alleviates cardiomyocyte senescence after MI. (**A**) Results of IHC staining for p21 and p53 in rat myocardial tissues from each group. Longitudinal section × 200, scale bar = 50 μm. (**B**) Results of β-Galactosidase staining of rat myocardial tissue from each group. Longitudinal section × 400, scale bar = 100 μm. (**C**) Quantitative analysis of the average optical density of p21 and p53 detected by IHC. (**D**) Quantitative analysis of the positive rate of β-Galactosidase staining. $^{\#\#}$ $P < 0.01$ compared with the sham-operated group; ^{ns} $P > 0.05$, * $P < 0.05$, and ** $P < 0.01$ compared with the model group ($\bar{x}\pm s$, n = 3).

lower in the GBE dosage groups than in the model group (Figure 8D and F). Additionally, the expression of p-PI3K, a gene downstream of CD28, along with AKT and NFκB phosphorylation, was significantly greater in the model group than in the sham-operated group. The phosphorylation of PI3K and AKT was significantly lower in the GBE dose groups than in the model group. Moreover, NFκB phosphorylation was significantly lower in the high-dose GBE group (Figure 8G and H). These findings suggest that ginkgetin may achieve cardioprotective effects by regulating the activation of the TCR signaling pathway, specifically by inhibiting the phosphorylation of CD3 and CD28. This mechanism supports the therapeutic role of ginkgetin in improving cardiac function post-MI.

Ginkgetin Alleviates OGD-Induced Senescent Apoptosis and Protects Cardiomyocytes

To assess the ability of ginkgetin to mitigate cytotoxicity, H9c2 cardiomyocytes were subjected to OGD to mimic myocardial ischemia. CCK8 and LDH assays of OGD-induced H9c2 cardiomyocytes revealed a significant decrease in cell viability and an increase in cytotoxicity after exposure to OGD. After 6 h of exposure to OGD, the cell viability decreased to 49.38 ±1.99%, and the mortality rate increased to 52.10 ±2.03%, establishing a suitable baseline for further experiments (Figure 9A and B). H9c2 cells were subsequently treated with various concentrations of ginkgetin for 6 h. The results of the CCK8 and LDH

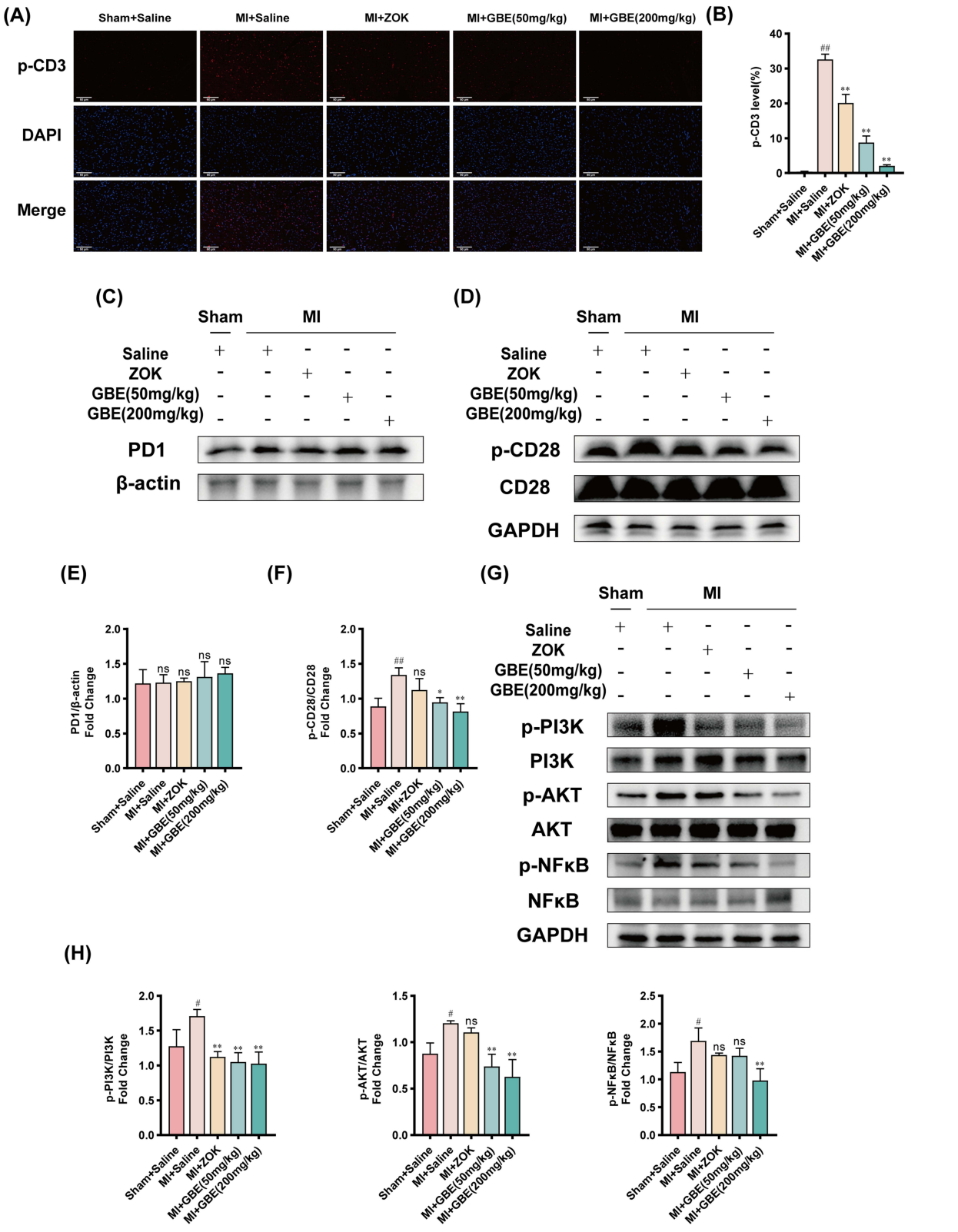

Figure 8 Ginkgetin modulates the activation of the T-cell signaling pathway for cardioprotection. (**A**) Immunofluorescence staining results of p-CD3 in the myocardial tissues of the rats in each group. Longitudinal section × 400, scale bar = 50 μm. (**B**) Quantitative analysis of p-CD3 fluorescence intensity. (**C**) WB bands showing PD-1 protein expression in the myocardial tissues of the rats in each group. (**D**) WB bands showing CD28 and p-CD28 protein expression in the myocardial tissues of the rats in each group. (**E**) Quantitative analysis of PD1 expression in each group. (**F**) Quantitative analysis of the p-CD28/CD28 ratio in each group. (**G**) WB bands showing p-PI3K, PI3K, p-AKT, AKT, p-NFκB, and NFκB protein expression in rat myocardial tissues from each group. (**H**) Quantitative analysis of the p-PI3K/PI3K ratio, p-AKT/AKT ratio, and p-NFκB/NFκB ratio in each group. Note: In (**E**), 'ns' indicates that no statistically significant difference in PD1 expression was detected between this group and any other group. Residual plots $^{\#}$ $P < 0.05$ and $^{\#\#}$ $P < 0.01$ compared with the sham-operated group; ^{ns} $P > 0.05$, * $P < 0.05$, and ** $P < 0.01$ compared with the model group ($\bar{x}\pm s$, n = 3).

https://doi.org/10.2147/JIR.S491535

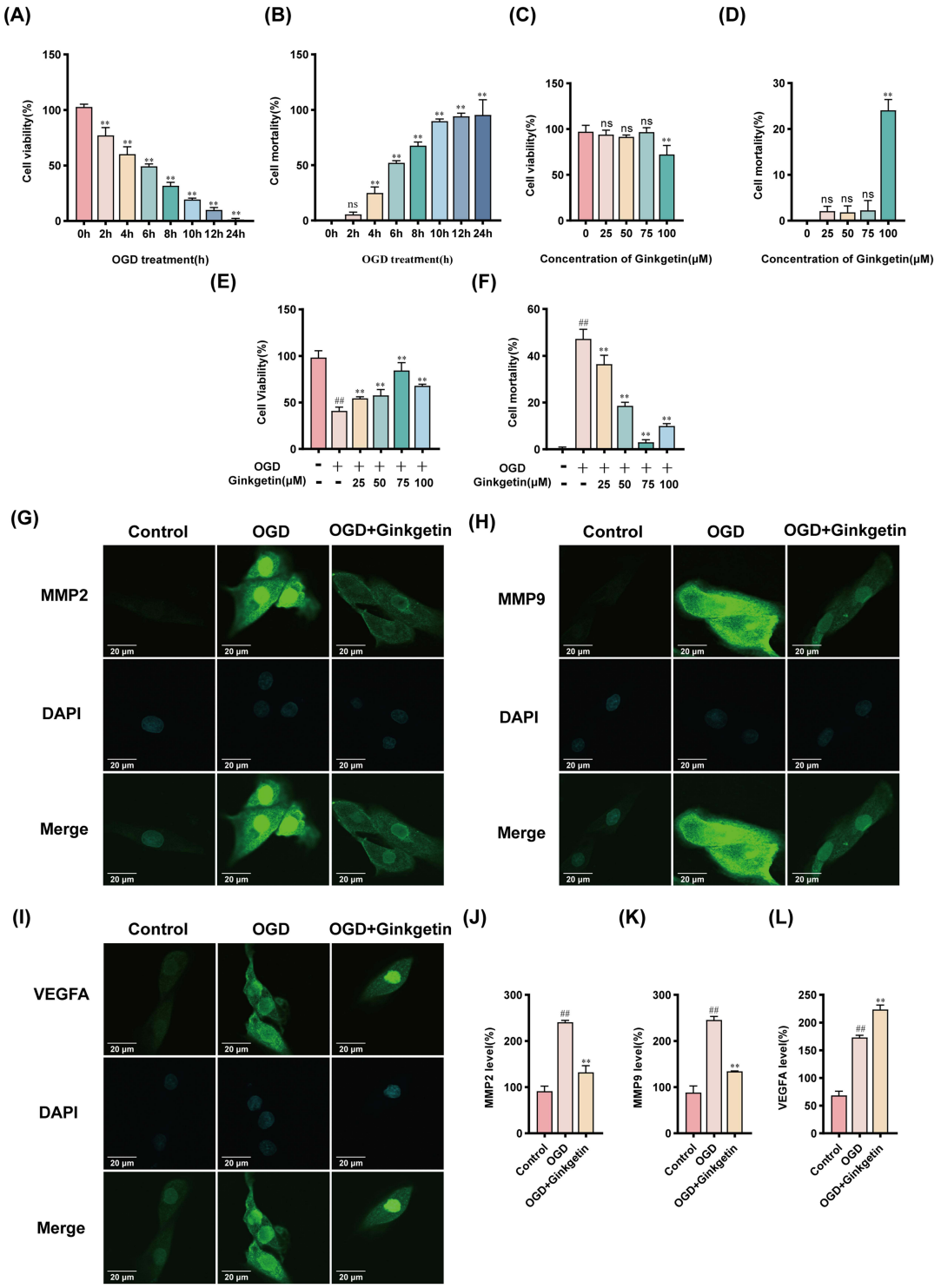

Figure 9 Ginkgetin attenuates elevated OGD-induced cytotoxicity, improves cell viability, and protects cardiomyocytes. (**A**) A CCK8 assay was performed to assess the viability of H9c2 cells exposed to OGD at different time points. (**B**) LDH release assays were performed to detect the cytotoxicity of H9c2 cells exposed to OGD at different time points. (**C**) A CCK8 assay was performed to detect the viability of H9c2 cells exposed to different concentrations of ginkgetin for 6 h. (**D**) LDH release assays were conducted to detect the cytotoxicity of different concentrations of ginkgetin to H9c2 cells after 6 h of treatment. (**E**) A CCK8 assay was conducted to detect the viability of H9c2 cells exposed to different concentrations of ginkgetin for 6 h under OGD conditions. (**F**) LDH release assays were conducted to detect the cytotoxicity of different concentrations of ginkgetin to H9c2 cells after 6 h of OGD treatment. (**G**) IF staining was performed for MMP2 in H9c2 cells from each group; 1200×; scale bar = 20 μm. (**H**) IF staining was performed for MMP9 in H9c2 cells from each group; 1200×; scale bar = 20 μm. (**I**) IF staining was performed for VEGFA in H9c2 cells in each group; 1200×; scale bar = 20 μm. (**J**) Quantitative analysis of MMP2 fluorescence intensity. (**K**) Quantitative analysis of MMP9 fluorescence intensity. (**L**) Quantitative analysis of VEGFA fluorescence intensity. For (**A-D**), ^{ns} $P > 0.05$ and ** $P < 0.01$ compared with the control group. Residual plots $^{\#\#}$ $P < 0.01$ compared with the control group; ** $P < 0.01$ compared with the OGD-treated group ($\bar{x}$±s, n = 3).

assays indicated that, compared with no treatment, treatment with ginkgetin at concentrations ranging from 25–75 μM did not significantly alter cell viability or cytotoxicity (Figure 9C and D). After treatment with OGD, the 75 μM ginkgetin-treated group demonstrated the strongest protection against OGD-induced damage (Figure 9E and F). To assess the protective effects of ginkgetin on H9c2 cardiomyocytes in vitro, the expression levels of the key target genes MMP2, MMP9, and VEGFA were examined through IF staining. The results revealed that the expression of MMP2 and MMP9 was significantly lower and that the expression of VEGFA was significantly greater in the ginkgetin-treated group than in the OGD group (Figure 9G–L). WB analysis, IF staining, and β-Galactosidase staining were subsequently conducted to determine whether ginkgetin could alleviate OGD-induced senescent apoptosis in cellular experiments. Compared with the OGD group, the ginkgetin-treated group presented lower expression of the apoptotic markers cleaved caspase 3 and Bax and higher expression of the anti-apoptotic marker Bcl-2 (Figure 10A and B). The results of IF staining revealed a significant reduction in the expression of the senescence markers p21 and p53 in the ginkgetin-treated group compared with the OGD group (Figure 10C–F). Similarly, β-Galactosidase staining indicated that ginkgetin administration significantly mitigated the cardiomyocyte senescence induced by OGD (Figure 10G and H). Therefore, ginkgetin significantly attenuated elevated OGD-induced cytotoxicity, increased cell viability, and alleviated OGD-induced senescent apoptosis, thus protecting cardiomyocytes.

Discussion

Previous studies on GBE have predominantly investigated its anti-inflammatory and anticoagulant properties, facilitating its extensive use in managing neurological disorders and peripheral vascular conditions. We performed DO enrichment analysis and found that ginkgetin can be enriched in atherosclerosis, suggesting its promising therapeutic role in CVD. Moreover, bioinformatics analysis revealed that the key targets of ginkgetin for MI treatment were MMP2, MMP9, and VEGFA. Immune infiltration analysis revealed that ginkgetin might be involved in immune regulation by acting on the TCR signaling pathway. Additionally, GO enrichment analysis revealed that ginkgetin might alleviate the senescent apoptosis of cardiomyocytes after MI by acting on the cell membrane to protect the heart. By conducting animal experiments, we found that ginkgetin exerts cardioprotective effects by inhibiting myocardial fibrosis and cardiomyocyte hypertrophy around the infarcted area after infarction, scavenging oxygen free radicals, attenuating postinfarction marginal cell inflammatory infiltration, inhibiting the activation of inflammatory-immune pathways, and delaying the occurrence of postinfarction peripheral cell senescent apoptosis. In vitro cellular experiments confirmed that ginkgetin significantly attenuated OGD-induced increased cytotoxicity, improved cell viability, and alleviated OGD-induced senescent apoptosis, thus protecting cardiomyocytes. Additionally, we preliminarily demonstrated that ginkgetin might regulate the activation of the TCR signaling pathway by inhibiting the phosphorylation of CD3 and CD28 on the surface of the T-cell membrane.

Several studies have shown that cardiomyocytes undergo "stress senescence" post-MI,[27] with senescent cells persistently affecting the surrounding microenvironment,[12] secreting inflammatory mediators and chemokines,[28] and recruiting immune cells to sustain inflammation.[29,30] Consequently, the inflammatory-immune pathway remains active, placing infarct border cells and even all ventricular cells in a state of immune infiltration. These changes further exacerbate senescent apoptosis in cardiomyocytes at the infarct border. We verified the immunomodulatory effects of ginkgetin in terms of inflammation, apoptosis, and senescence. H&E staining revealed that cardiomyocyte edema and inflammatory infiltration were significantly reduced in MI model rats in each GBE dose group. The ELISA results revealed that each GBE dose significantly decreased the expression of the inflammatory factors IL-6, IL-1β, and TNF-α and attenuated inflammatory infiltration. TUNEL staining and WB analysis indicated that high-dose GBE had high anti-apoptotic efficacy. IHC and β-Galactosidase staining suggested that high-dose GBE considerably delayed cardiomyocyte senescence. The results of the cellular experiments confirmed that ginkgetin alleviated OGD-induced senescence and apoptosis. MI leads to the transformation of cardiac fibroblasts into myofibroblasts,[31] which secrete large amounts of extracellular matrix proteins (ECMs),[32] replacing most of the myocardium with dense collagen fibers after MI.[33] Masson and Sirius Red staining indicated that the GBE extracts in all the GBE dose groups significantly decreased collagen fiber deposition. Mitochondrial dysfunction, which leads to an increase in ROS production and oxidative stress damage,[34] promotes cellular senescence.[35] Overproduction of ROS further exacerbates structural damage to mitochondria in injured cardiomyocytes;[36] thus, some researchers have proposed targeting mitochondria to scavenge ROS, attenuate

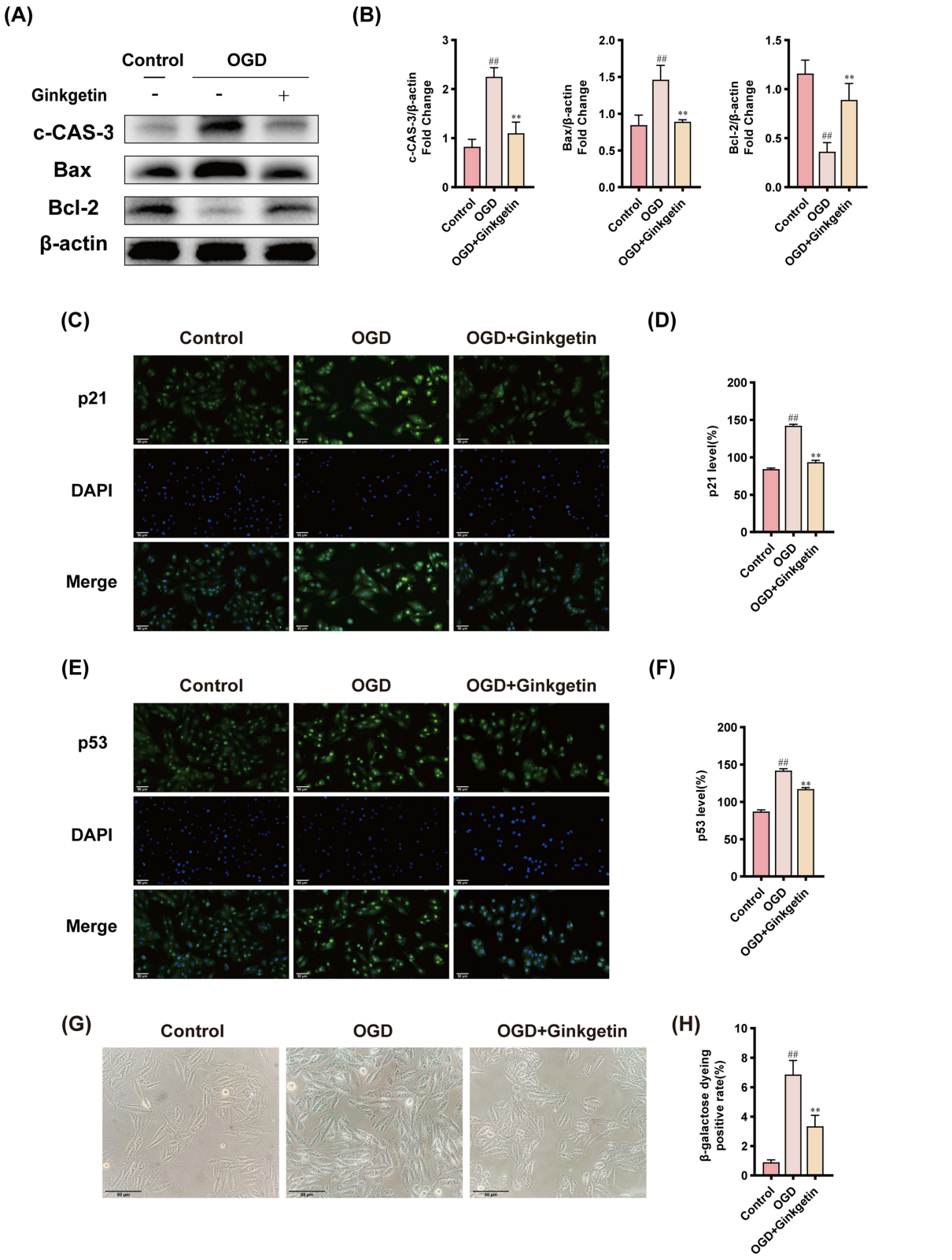

Figure 10 Ginkgetin alleviates OGD-induced senescent apoptosis. (**A**) WB bands showing cleaved caspase 3, Bax, and Bcl-2 protein expression in H9c2 cardiomyocytes from each group. (**B**) Quantitative analysis of cleaved caspase 3, Bax, and Bcl-2 expression in each group. (**C**) IF staining was performed for p21 in H9c2 cells from each group; 400×; scale bar = 50 μm. (**D**) Quantitative analysis of p21 fluorescence intensity. (**E**) IF staining was performed for p53 in H9c2 cells from each group; 400×; scale bar = 50 μm. (**F**) Quantitative analysis of p53 fluorescence intensity. (**G**) Results of β-Galactosidase staining of H9c2 cardiomyocytes from each group; 400×; scale bar = 50 μm. (**H**) Quantitative analysis of β-Galactosidase staining positivity. $^{\#\#}P < 0.01$ compared with the blank control group; $^{**}P < 0.01$ compared with the OGD-treated group ($\bar{x}\pm s$, n = 3).

https://doi.org/10.2147/JIR.S491535

inflammatory infiltration, and improve mitochondrial morphology and function to alleviate myocardial fibrosis.[37] Our TEM results revealed a significant improvement in the mitochondrial microstructure across all the GBE dose groups. ROS fluorescence staining also revealed a significant reduction in mitochondrial ROS production in cardiomyocytes treated with GBE.

Matrix metalloproteinases (MMPs) play crucial roles in the degradation of extracellular matrix proteins, and their overactivation leads to cardiomyocyte slippage and loss of cardiac homeostasis.[38] Post-MI, MMPs recruit immune cells to clear necrotic and senescent cardiomyocytes, which, along with recruited immune cells, release different types of proinflammatory factors, triggering extensive activation of MMPs,[39] accelerating myocardial structural changes, and leading to dysfunctional myocardial remodeling.[40] VEGFA, a vascular endothelial growth factor, enhances angiogenesis at the lesion site post-MI, facilitating collateral circulation to meet the blood supply demand of the heart.[41] Transient expression of the VEGF gene can prevent the enlargement of infarcts and ventricular remodeling post-MI.[42] The results of our WB, RT-qPCR, and cellular immunofluorescence assays revealed a significant decrease in MMP2 and MMP9 expression and an increase in VEGFA expression in the GBE dose groups and the ginkgetin treatment groups.

T cells, critical leukocytes in the immune response, recognize cell membrane surface antigens via the TCR and stimulate an immune response.[43] Under normal circumstances, innate and adaptive immune cells maintain homeostasis. After MI, T cells migrate as adaptive immune cells from the blood to diseased tissue, where immune infiltration can maintain cardiac homeostasis.[44,45] However, the post-MI accumulation of senescent cells in vivo triggers the release of different types of inflammatory factors, disrupting immune homeostasis and leading to excessive activation of the TCR signaling pathway. The TCRα/β heterodimer in the T-cell membrane couples with the CD3 complex to form the TCR-CD3 complex, and the binding of antigens to TCR-αβ results in the phosphorylation of CD3 ITAMs, thus transmitting activation signals.[46] We found that GBE significantly decreased the phosphorylation level of CD3 across all dosage groups. Programmed cell death protein 1 (PD1), a co-inhibitory receptor found on the surface of T cells, is predominantly expressed in nonfunctional and exhausted T cells,[47] making targeting PD1 a popular cancer treatment strategy.[48] CD28 acts as a co-stimulatory receptor in T cells, where the phosphorylation of CD28 YMNM motifs recruits PI3K. The activation of PI3K leads to the downstream phosphorylation of AKT and nuclear factor inhibitor κB (IκB). This causes NFκB to be released from the IκB complex in the cytoplasm and subsequently translocate into the nucleus to regulate gene expression.[49] Our findings revealed no significant differences in PD1 expression across groups; however, the levels of p-CD28, p-PI3K, p-AKT, and p-NFκB were significantly reduced in the GBE treatment groups. Thus, it is highly plausible that ginkgetin modulates the activation of the TCR signaling pathway by dephosphorylating CD3 and CD28.

To summarize, our results confirmed that ginkgetin can delay senescent apoptosis and provide cardioprotection to infarct border cells after MI. The effects of ginkgetin were most likely achieved by dephosphorylating CD3 and CD28 to downregulate the activation signals of the TCR signaling pathway.

Data Sharing Statement

Publicly available datasets (GSE34198, GSE48060, GSE97320) were analyzed in this study. The dataset was obtained from the GEO (http://www.ncbi.nlm.nih.gov/geo) database.

Ethics Approval

The animal study was reviewed and approved by the Ethics Committee of Liaoning University of Traditional Chinese Medicine. All public databases involving human data have undergone review and approval by the Ethics Committee of the Affiliated Hospital of Liaoning University of Traditional Chinese Medicine.

Acknowledgments

We are very grateful to the GEO database for providing meaningful datasets. The graphical abstract was created in BioRender. Li, H. (2024) https://BioRender.com/f73a336.

Author Contributions

All authors made a significant contribution to the work reported, whether that is in the conception, study design, execution, acquisition of data, analysis and interpretation, or in all these areas; took part in drafting, revising or critically reviewing the article; gave final approval of the version to be published; have agreed on the journal to which the article has been submitted; and agree to be accountable for all aspects of the work.

Funding

This work was supported by the Young Qihuang Scholars Support Project of the State Administration of Traditional Chinese Medicine (20201A2180) and the Liaoning Provincial Science and Technology Programme Joint Programme (Fund) Project(2023-MSLH-191).

Disclosure

The authors declare that the research was conducted in the absence of any commercial or financial relationships that could be construed as a potential conflict of interest.

References

1. Jortveit J, Pripp AH, Langorgen J, Halvorsen S. Incidence, risk factors and outcome of young patients with myocardial infarction. *Heart*. 2020;106(18):1420–1426. doi:10.1136/heartjnl-2019-316067
2. Moraes-Silva IC, Rodrigues B, Coelho-Junior HJ, Feriani DJ, Irigoyen MC. Myocardial infarction and exercise training: evidence from basic science. *Adv Exp Med Biol*. 2017;999:139–153.
3. Smolderen KG, Brush A, Dreyer RP. Psychosocial factors and recovery after acute myocardial infarction in younger women. *Curr Cardiol Rep*. 2019;21(6):50. doi:10.1007/s11886-019-1140-x
4. Collet JP, Thiele H, Barbato E, et al. 2020 ESC Guidelines for the management of acute coronary syndromes in patients presenting without persistent ST-segment elevation. *Eur Heart J*. 2021;42(14):1289–1367. doi:10.1093/eurheartj/ehaa575
5. Samsky MD, Morrow DA, Proudfoot AG, Hochman JS, Thiele H, Rao SV. Cardiogenic shock after acute myocardial infarction: a review. *JAMA*. 2021;326(18):1840–1850. doi:10.1001/jama.2021.18323
6. Frangogiannis NG. Pathophysiology of myocardial infarction. *Compr Physiol*. 2015;5(4):1841–1875.
7. Birch J, Gil J. Senescence and the SASP: many therapeutic avenues. *Genes Dev*. 2020;34(23–24):1565–1576. doi:10.1101/gad.343129.120
8. Acosta JC, O'Loghlen A, Banito A, et al. Chemokine signaling via the CXCR2 receptor reinforces senescence. *Cell*. 2008;133(6):1006–1018. doi:10.1016/j.cell.2008.03.038
9. Takahashi A, Loo TM, Okada R, et al. Downregulation of cytoplasmic DNases is implicated in cytoplasmic DNA accumulation and SASP in senescent cells. *Nat Commun*. 2018;9(1):1249. doi:10.1038/s41467-018-03555-8
10. Takasugi M, Yoshida Y, Ohtani N. Cellular senescence and the tumour microenvironment. *Mol Oncol*. 2022;16(18):3333–3351. doi:10.1002/1878-0261.13268
11. Dookun E, Walaszczyk A, Redgrave R, et al. Clearance of senescent cells during cardiac ischemia-reperfusion injury improves recovery. *Aging Cell*. 2020;19(10):e13249. doi:10.1111/acel.13249
12. Khavinson V, Linkova N, Dyatlova A, Kantemirova R, Kozlov K. Senescence-associated secretory phenotype of cardiovascular system cells and inflammaging: perspectives of peptide regulation. *Cells*. 2022;12(1):106. doi:10.3390/cells12010106
13. Carrillo-Salinas FJ, Ngwenyama N, Anastasiou M, Kaur K, Alcaide P. Heart inflammation: immune cell roles and roads to the heart. *Am J Pathol*. 2019;189(8):1482–1494. doi:10.1016/j.ajpath.2019.04.009
14. Pinti M, Appay V, Campisi J, et al. Aging of the immune system: focus on inflammation and vaccination. *European J Immunol*. 2016;46(10):2286–2301. doi:10.1002/eji.201546178
15. Sun L, Wang X, Saredy J, Yuan Z, Yang X, Wang H. Innate-adaptive immunity interplay and redox regulation in immune response. *Redox Biol*. 2020;37:101759. doi:10.1016/j.redox.2020.101759
16. Xu HY, Zhang YQ, Liu ZM, et al. ETCM: an encyclopaedia of traditional Chinese medicine. *Nucleic Acids Res*. 2019;47(D1):D976–d982. doi:10.1093/nar/gky987
17. Barker CS, Elston DM. Botanical briefs: ginkgo (Ginkgo biloba). *Cutis*. 2022;110(1):30–33. doi:10.12788/cutis.0559
18. Tsai HY, Huang PH, Lin FY, Chen JS, Lin SJ, Chen JW. Ginkgo biloba extract reduces high-glucose-induced endothelial reactive oxygen species generation and cell adhesion molecule expression by enhancing HO-1 expression via Akt/eNOS and p38 MAP kinase pathways. *European J Pharmaceut Sci*. 2013;48(4–5):803–811. doi:10.1016/j.ejps.2013.01.002
19. Liu L, Wang Y, Zhang J, Wang S. Advances in the chemical constituents and chemical analysis of Ginkgo biloba leaf, extract, and phytopharmaceuticals. *J Pharmaceut Biomed Analys*. 2021;193:113704. doi:10.1016/j.jpba.2020.113704
20. Lian N, Tong J, Li W, Wu J, Li Y. Ginkgetin ameliorates experimental atherosclerosis in rats. *Biomed Pharmacother*. 2018;102:510–516. doi:10.1016/j.biopha.2018.03.107
21. Cho YL, Park JG, Kang HJ, et al. Ginkgetin, a biflavone from Ginkgo biloba leaves, prevents adipogenesis through STAT5-mediated PPARγ and C/EBPα regulation. *Pharmacol Res*. 2019;139:325–336. doi:10.1016/j.phrs.2018.11.027
22. Liu Y, Ye J, Fan Z, et al. Ginkgetin alleviates inflammation and senescence by targeting STING. *Adv Sci*. 2024:e2407222. doi:10.1002/advs.202407222
23. Zhao S, Wu Y, Wei Y, Xu X, Zheng J. Identification of biomarkers associated with CD8+ T cells in coronary artery disease and their pan-cancer analysis. *Front Immunol*. 2022;13:876616. doi:10.3389/fimmu.2022.876616

24. Suresh R, Li X, Chiriac A, et al. Transcriptome from circulating cells suggests dysregulated pathways associated with long-term recurrent events following first-time myocardial infarction. *J Mol Cell Cardiol*. 2014;74:13–21. doi:10.1016/j.yjmcc.2014.04.017
25. Zhang N, Zhou B, Tu S. Identification of an 11 immune-related gene signature as the novel biomarker for acute myocardial infarction diagnosis. *Genes Immun*. 2022;23(7):209–217. doi:10.1038/s41435-022-00183-7
26. Saul D, Kosinsky RL, Atkinson EJ, et al. A new gene set identifies senescent cells and predicts senescence-associated pathways across tissues. *Nat Commun*. 2022;13(1):4827. doi:10.1038/s41467-022-32552-1
27. Banerjee P, Kotla S, Reddy Velatooru L, et al. Senescence-associated secretory phenotype as a hinge between cardiovascular diseases and cancer. *Front Cardiovasc Med*. 2021;8:763930. doi:10.3389/fcvm.2021.763930
28. Mehdizadeh M, Aguilar M, Thorin E, Ferbeyre G, Nattel S. The role of cellular senescence in cardiac disease: basic biology and clinical relevance. *Nat Rev Cardiol*. 2022;19(4):250–264. doi:10.1038/s41569-021-00624-2
29. Lopes-Paciencia S, Saint-Germain E, Rowell MC, Ruiz AF, Kalegari P, Ferbeyre G. The senescence-associated secretory phenotype and its regulation. *Cytokine*. 2019;117:15–22. doi:10.1016/j.cyto.2019.01.013
30. Teissier T, Boulanger E, Cox LS. Interconnections between Inflammageing and Immunosenescence during Ageing. *Cells*. 2022;11(3). doi:10.3390/cells11030359
31. Venugopal H, Hanna A, Humeres C, Frangogiannis NG. Properties and functions of fibroblasts and myofibroblasts in myocardial infarction. *Cells*. 2022;11(9):1386. doi:10.3390/cells11091386
32. Sun Y, Ma M, Cao D, et al. Inhibition of Fap promotes cardiac repair by stabilizing BNP. *Circulation Res*. 2023;132(5):586–600. doi:10.1161/CIRCRESAHA.122.320781
33. Sosnovik DE, Mekkaoui C, Huang S, et al. Microstructural impact of ischemia and bone marrow-derived cell therapy revealed with diffusion tensor magnetic resonance imaging tractography of the heart in vivo. *Circulation*. 2014;129(17):1731–1741. doi:10.1161/CIRCULATIONAHA.113.005841
34. Chen MS, Lee RT, Garbern JC. Senescence mechanisms and targets in the heart. *Cardiovasc Res*. 2022;118(5):1173–1187. doi:10.1093/cvr/cvab161
35. Vasileiou PVS, Evangelou K, Vlasis K, et al. Mitochondrial homeostasis and cellular senescence. *Cells*. 2019;8(7):686. doi:10.3390/cells8070686
36. Shadel GS, Horvath TL. Mitochondrial ROS signaling in organismal homeostasis. *Cell*. 2015;163(3):560–569. doi:10.1016/j.cell.2015.10.001
37. Wang J, Chen P, Cao Q, Wang W, Chang X. Traditional Chinese medicine ginseng dingzhi decoction ameliorates myocardial fibrosis and high glucose-induced cardiomyocyte injury by regulating intestinal flora and mitochondrial dysfunction. *Oxid Med Cell Longev*. 2022;2022:9205908. doi:10.1155/2022/9205908
38. Ibarra-Lara L, Sánchez-Aguilar M, Soria-Castro E, et al. Clofibrate treatment decreases inflammation and reverses myocardial infarction-induced remodelation in a rodent experimental model. *Molecules*. 2019;24(2):270. doi:10.3390/molecules24020270
39. DeLeon-Pennell KY, Meschiari CA, Jung M, Lindsey ML. Matrix metalloproteinases in myocardial infarction and heart failure. *Progress Molecular Biol Translat Sci*. 2017;147:75–100.
40. Liu D, Guo M, Zhou P, Xiao J, Ji X. TSLP promote M2 macrophages polarization and cardiac healing after myocardial infarction. *Biochem Biophys Res Commun*. 2019;516(2):437–444. doi:10.1016/j.bbrc.2019.06.041
41. Zou J, Fei Q, Xiao H, et al. VEGF-A promotes angiogenesis after acute myocardial infarction through increasing ROS production and enhancing ER stress-mediated autophagy. *J Cell Physiol*. 2019;234(10):17690–17703. doi:10.1002/jcp.28395
42. Matsumoto R, Omura T, Yoshiyama M, et al. Vascular endothelial growth factor-expressing mesenchymal stem cell transplantation for the treatment of acute myocardial infarction. *Arteriosclerosis Thrombosis Vasc Biol*. 2005;25(6):1168–1173. doi:10.1161/01.ATV.0000165696.25680.ce
43. Saravia J, Raynor JL, Chapman NM, Lim SA, Chi H. Signaling networks in immunometabolism. *Cell Res*. 2020;30(4):328–342. doi:10.1038/s41422-020-0301-1
44. Rossy J, Laufer JM, Legler DF. Role of mechanotransduction and tension in T cell function. *Front Immunol*. 2018;9:2638. doi:10.3389/fimmu.2018.02638
45. Zhuang L, Wang Y, Chen Z, et al. Global characteristics and dynamics of single immune cells after myocardial infarction. *J Am Heart Assoc*. 2022;11(24):e027228. doi:10.1161/JAHA.122.027228
46. Ngoenkam J, Schamel WW, Pongcharoen S. Selected signalling proteins recruited to the T-cell receptor-CD3 complex. *Immunology*. 2018;153(1):42–50. doi:10.1111/imm.12809
47. McKinney EF, Lee JC, Jayne DR, Lyons PA, Smith KG. T-cell exhaustion, co-stimulation and clinical outcome in autoimmunity and infection. *Nature*. 2015;523(7562):612–616. doi:10.1038/nature14468
48. Cristescu R, Mogg R, Ayers M, et al. Pan-tumor genomic biomarkers for PD-1 checkpoint blockade-based immunotherapy. *Science*. 2018;362(6411). doi:10.1126/science.aar3593
49. Honikel MM, Olejniczak SH. Co-stimulatory receptor signaling in CAR-T cells. *Biomolecules*. 2022;12(9):1303. doi:10.3390/biom12091303

Journal of Inflammation Research

Dovepress
Taylor & Francis Group

Publish your work in this journal

The Journal of Inflammation Research is an international, peer-reviewed open-access journal that welcomes laboratory and clinical findings on the molecular basis, cell biology and pharmacology of inflammation including original research, reviews, symposium reports, hypothesis formation and commentaries on: acute/chronic inflammation; mediators of inflammation; cellular processes; molecular mechanisms; pharmacology and novel anti-inflammatory drugs; clinical conditions involving inflammation. The manuscript management system is completely online and includes a very quick and fair peer-review system. Visit http://www.dovepress.com/testimonials.php to read real quotes from published authors.

Submit your manuscript here: https://www.dovepress.com/journal-of-inflammation-research-journal